Cell Reports
Medicine

Article

# Targeted therapy improves cellular dysfunction, ataxia, and seizure susceptibility in a model of a progressive myoclonus epilepsy

## Graphical abstract

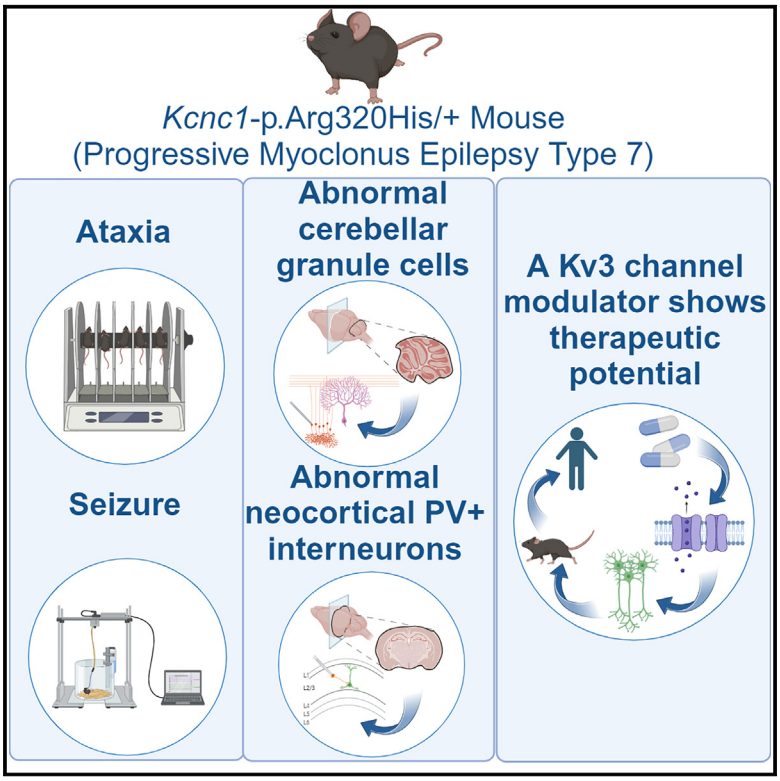


## Authors

Huijie Feng, Jerome Clatot, Keisuke Kaneko, ..., Charles H. Large, Naiara Akizu, Ethan M. Goldberg

## Correspondence

goldberge@chop.edu

## In brief

The Arg320His variant in *KCNC1* encoding the potassium channel subunit Kv3.1 causes progressive myoclonus epilepsy type 7. Feng et al. generate a mouse model (*Kcnc1*-p.Arg320His/+ mice), and a Kv3 channel positive modulator improves dysfunction of Kv3.1-expressing neurons *in vitro* and motor impairment and seizure susceptibility in *Kcnc1*-p.Arg320His/+ mice *in vivo.*

## Highlights

- *KCNC1* encodes the voltage-gated potassium channel subunit Kv3.1
- The variant *KCNC1*-R320H causes progressive myoclonus epilepsy type 7 (EPM7)
- *Kcnc1*-R320H/+ mice recapitulate the core EPM7 phenotype
- A Kv3 modulator improves motor function and seizure susceptibility in H/+ mice *in vivo*

Feng et al., 2024, Cell Reports Medicine *5*, 101389
February 20, 2024 
https://doi.org/10.1016/j.xcrm.2023.101389

CellPress

Cell Reports Medicine

CellPress
OPEN ACCESS

Article

# Targeted therapy improves cellular dysfunction, ataxia, and seizure susceptibility in a model of a progressive myoclonus epilepsy

Huijie Feng,[1] Jerome Clatot,[1,2] Keisuke Kaneko,[1,10] Marco Flores-Mendez,[3] Eric R. Wengert,[1] Carly Koutcher,[1] Emily Hoddeson,[1] Emily Lopez,[4] Demetrius Lee,[1] Leroy Arias,[4] Qiansheng Liang,[5] Xiaohong Zhang,[1] Ala Somarowthu,[1] Manuel Covarrubias,[5] Martin J. Gunthorpe,[6] Charles H. Large,[6] Naiara Akizu,[3,7] and Ethan M. Goldberg[1,2,8,9,11,*]

[1]Division of Neurology, Department of Pediatrics, The Children's Hospital of Philadelphia, Philadelphia, PA 19104, USA
[2]The Epilepsy Neurogenetics Initiative, The Children's Hospital of Philadelphia, Philadelphia, PA 19104, USA
[3]The Raymond G. Perelman Center for Cellular and Molecular Therapeutics, The Children's Hospital of Philadelphia, Philadelphia, PA 19104, USA
[4]The University of Pennsylvania School of Arts and Sciences, Philadelphia, PA, USA
[5]Department of Neuroscience and Vickie and Jack Farber Institute for Neuroscience, Sidney Kimmel Medical College at Thomas Jefferson University, Philadelphia, PA 19107, USA
[6]Autifony Therapeutics, Ltd., Stevenage Bioscience Catalyst, Stevenage SG1 2FX, UK
[7]Departments of Pathology & Laboratory Medicine, The University of Pennsylvania Perelman School of Medicine, Philadelphia, PA 19104, USA
[8]Department of Neurology, The University of Pennsylvania Perelman School of Medicine, Philadelphia, PA 19104, USA
[9]Department of Neuroscience, The University of Pennsylvania Perelman School of Medicine, Philadelphia, PA 19104, USA
[10]Department of Anesthesiology, Nihon University, 1-8-13 Kanda-Surugadai, Chiyoda-ku, Tokyo 101-8310, Japan
[11]Lead contact
*Correspondence: goldberge@chop.edu
https://doi.org/10.1016/j.xcrm.2023.101389

## SUMMARY

The recurrent variant *KCNC1*-p.Arg320His causes progressive myoclonus epilepsy (EPM) type 7, defined by progressive myoclonus, epilepsy, and ataxia, and is without effective treatment. *KCNC1* encodes the voltage-gated potassium channel subunit Kv3.1, specifically expressed in high-frequency-firing neurons. Variant subunits act via loss of function; hence, EPM7 pathogenesis may involve impaired excitability of Kv3.1-expressing neurons, while enhancing Kv3 activity could represent a viable therapeutic strategy. We generate a mouse model, *Kcnc1*-p.Arg320His/+, which recapitulates the core features of EPM7, including progressive ataxia and seizure susceptibility. Kv3.1-expressing cerebellar granule cells and neocortical parvalbumin-positive GABAergic interneurons exhibit abnormalities consistent with Kv3 channel dysfunction. A Kv3-specific positive modulator (AUT00206) selectively enhances the firing frequency of Kv3.1-expressing neurons and improves motor function and seizure susceptibility in *Kcnc1*-Arg320His/+ mice. This work identifies a cellular and circuit basis of dysfunction in EPM7 and demonstrates that Kv3 positive modulators such as AUT00206 have therapeutic potential for the treatment of EPM7.

## INTRODUCTION

A recurrent heterozygous variant in *KCNC1*, which encodes the voltage-gated potassium (K+) channel subunit Kv3.1, was recently identified as the cause of progressive myoclonus epilepsy type 7 (EPM7; PME7), also known as myoclonus epilepsy and ataxia due to *KCNC1* mutation (MEAK).[1–3] EPM is a collection of disorders characterized by epilepsy and progressive myoclonus along with tremor and ataxia, loss of ambulation, and relentless neurological decline.[1,4] The 15+ EPMs are each associated with a defined genetic or metabolic etiology.[4] In general, mechanisms of EPM have been difficult to address due to the nature of the causative genes, lack of appropriate experimental models that reproduce salient aspects of these disorders, and lack of small molecules that target putative disease pathomechanisms. Treatment is symptomatic and not mechanistically oriented toward the underlying genetic defect. Current therapy involves standard anti-seizure medications, which do not address the underlying pathophysiology, are minimally effective at controlling symptoms, and have no influence on long-term disease course.[5–7] For EPM7, patients develop symptoms between the ages of 6 and 14 years,[1,3] with predominant myoclonus and ataxia that progressively worsens such that patients are wheelchair bound by adolescence or early adulthood and retain minimal functional limb use.

EPM7 is autosomal dominant, caused by the recurrent heterozygous variant *KCNC1*-p.Arg320His occurring either *de novo* or (less frequently) inherited from an affected parent

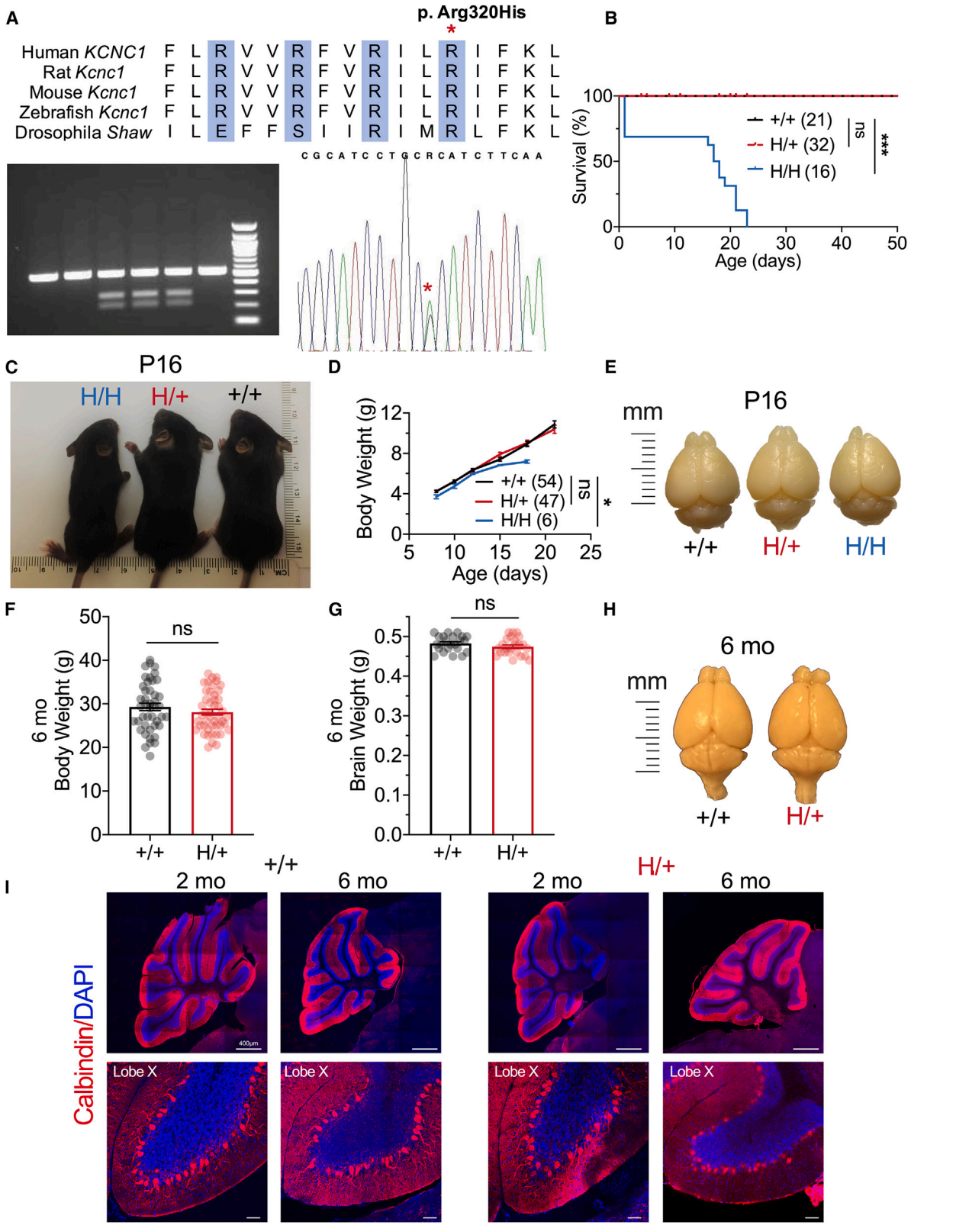


*(legend on next page)*

(impacting one of the two copies of *KCNC1*).[2] K+ channels are organized into families and subfamilies based on DNA sequence similarity,[8,9] and the variety of over 70 K+ channel genes are important regulators of neuronal excitability, while genetic variation is a known cause of epilepsy and other neurological disorders.[10–13] Kv3.1 is a member of the Kv3 subfamily of voltage-gated K+ channels, and Kv3 channels exist as heterotetrameric assemblies of Kv3.1–Kv3.4 subunits.[14–16] The recurrent EPM7-associated pathogenic variant *KCNC1*-p.Arg320His is localized to the fourth of the highly conserved positively charged arginine residues of the Kv subunit S4 voltage sensor; this variant causes loss of function with a putative dominant-negative effect,[2,3] and forms heteromultimers with wild-type Kv3.1 (and likely Kv3.2, Kv3.3, and/or Kv3.4),[9,14,16,17] to reduce Kv3 channel activity. Kv3.1 protein is abundantly expressed in discrete brain areas and in specific cell types that fire action potentials at high frequency, including in a subset of GABAergic inhibitory interneurons in the neocortex, hippocampus, and striatum, neurons of the reticular thalamic nucleus and auditory brainstem, and granule cells and molecular layer interneurons of the cerebellum.[14,18] Kv3.1 in the cerebral cortex is prominently and specifically expressed in parvalbumin (PV)-positive GABAergic fast-spiking interneurons (PV-INs) and underlies the ability of these cells to discharge at high frequency,[19–23] based on the distinct biophysical properties of the Kv3 subfamily among Kv subunits. Kv3.1-containing channels exhibit a uniquely positive (depolarized) voltage dependence of activation (with a $V_{1/2}$ of +15 mV) such that the outward K+ current does not "compete" with the inward sodium current driving the upswing of the action potential. Kv3.1 has rapid activation and deactivation kinetics, which facilitates repolarization of the action potential to keep spikes brief while driving a fast, deep afterhyperpolarization that facilitates recovery from the inactivation of Na+ channels and thereby limits the interspike interval.[20,24] Hence, loss-of-function variants of *KCNC1* would be expected to impair high-frequency firing of Kv3.1-expressing neurons. Importantly, Kv3.1-subunit-containing K+ channels are also expressed at synapses, where they modulate the presynaptic action potential waveform and thus influence transmitter release, regulating synaptic strength and short-term synaptic plasticity via regulation of spike width and spike-evoked calcium influx.[17,21,25,26] Again, loss-of-function variants would be expected to impact the dynamics of neurotransmitter release by Kv3.1-expressing neurons.

Here, we hypothesize that the complex clinical features of EPM7 are due to dysfunction of Kv3.1-expressing neurons in distributed brain regions. Specifically, we predict that susceptibility to seizure may be due to expression of dysfunctional Kv3.1-p.Arg320His subunits in PV-INs in the cerebral cortex, while ataxia may relate to dysfunction of affected cerebellar circuits. Augmenting Kv3 currents in affected cell populations could recover function and would represent a targeted treatment for EPM7.

We generated a preclinical experimental mouse model of EPM7 via CRIPSR-Cas9: *Kcnc1*-p.Arg320His/+ (H/+) mice are viable but show impairments across a battery of tests of motor function and exhibit a heightened susceptibility to induced seizure as well as the presence of spontaneous seizures. Kv3.1-expressing cerebellar granule cells and neocortical PV-INs show impaired excitability in acute brain slices from H/+ mice, specifically with respect to parameters consistent with Kv3 channel dysfunction. Application of a Kv3-specific K+ channel modulator, AUT00206, augments action potential generation *in vitro*, while injection of AUT00206 *in vivo* enhances motor performance and improves seizure susceptibility of H/+ mice.

These results identify cellular- and circuit-level mechanisms of EPM7 and suggest a targeted therapeutic approach that could be translated to treatment of human patients with EPM7 and potentially other phenotypically similar forms of EPM.

## RESULTS

### A mouse model of EPM7

We generated a mouse model, H/+ mice—homologous to the recurrent heterozygous variant *KCNC1* c.959G>A (p.Arg320His) identified in patients with EPM7—using CRISPR-Cas9 (Figure 1). There is extensive sequence similarity between mouse *Kcnc1* and human *KCNC1* including Arg320, the fourth positively charged arginine of the highly conserved S4 voltage sensor of Kv channels (Figure 1A). We performed detailed off-target analysis of multiple mosaic lines to confirm specificity of the mutation given the sequence similarity between Kv3 subfamily members *Kcnc1-4* and confirmed the selective editing of *Kcnc1* c.959G>A. Mice were then bred onto a C57BL/6J background for at least ten

**Figure 1. A mouse model of progressive myoclonus epilepsy type 7**

(A) Sequence similarity between mouse *Kcnc1* and human *KCNC1* including the Arg320 residue (asterisk), which constitutes the fourth positively charged arginine residue of the highly conserved S4 voltage sensor of Kv channels.

(B) Survival of wild-type (+/+ mice, n = 21), heterozygous (H/+ [*Kcnc1*-p.Arg320His/+] mice, n = 32), and homozygous (H/H mice: n = 18) mice.

(C) Representative image of +/+, H/+, and H/H mice at P16. Note the normal size of H/+ relative to +/− mice, with a growth impairment of the H/H mice.

(D) H/H mice are smaller compared to age-matched +/+ and H/+ littermates, while there is no significant weight difference between +/+ and H/+ mice at or before weaning. +/+ mice, n = 54; H/+ mice, n = 47; H/H mice, n = 6.

(E) Representative image demonstrates normal brain size between genotypes at P16.

(F and G) There is no difference between +/+ and H/+ mice in body weight (F) or brain weight (G) at 6 months of age. (F) +/+ mice, n = 30; H/+ mice, n = 29. (G) +/+ mice, n = 23; H/+ mice, n = 24. Data are separated by sex in Figure S2.

(H) Representative image of +/+ and H/+ mouse brains at 6 months of age.

(I) Confocal images of calbindin (a marker of Purkinje cells; red) and DAPI (blue) staining in cerebellum demonstrates normal gross anatomy and cytoarchitecture between +/+ and H/+ mice at 2 and 6 months of age. Scale bars: 400 μm (top) and 50 μm (bottom). See also Figures S2, S3, and S5 and Table S1. Data are presented as mean ± SEM.

Statistical analyses: Mantel-Cox test (B), two-way ANOVA with Šídák's multiple comparison test (D), and unpaired Student's t test (F and G). *p < 0.05 and ***p < 0.001. Exact p values can be found in Table S1.

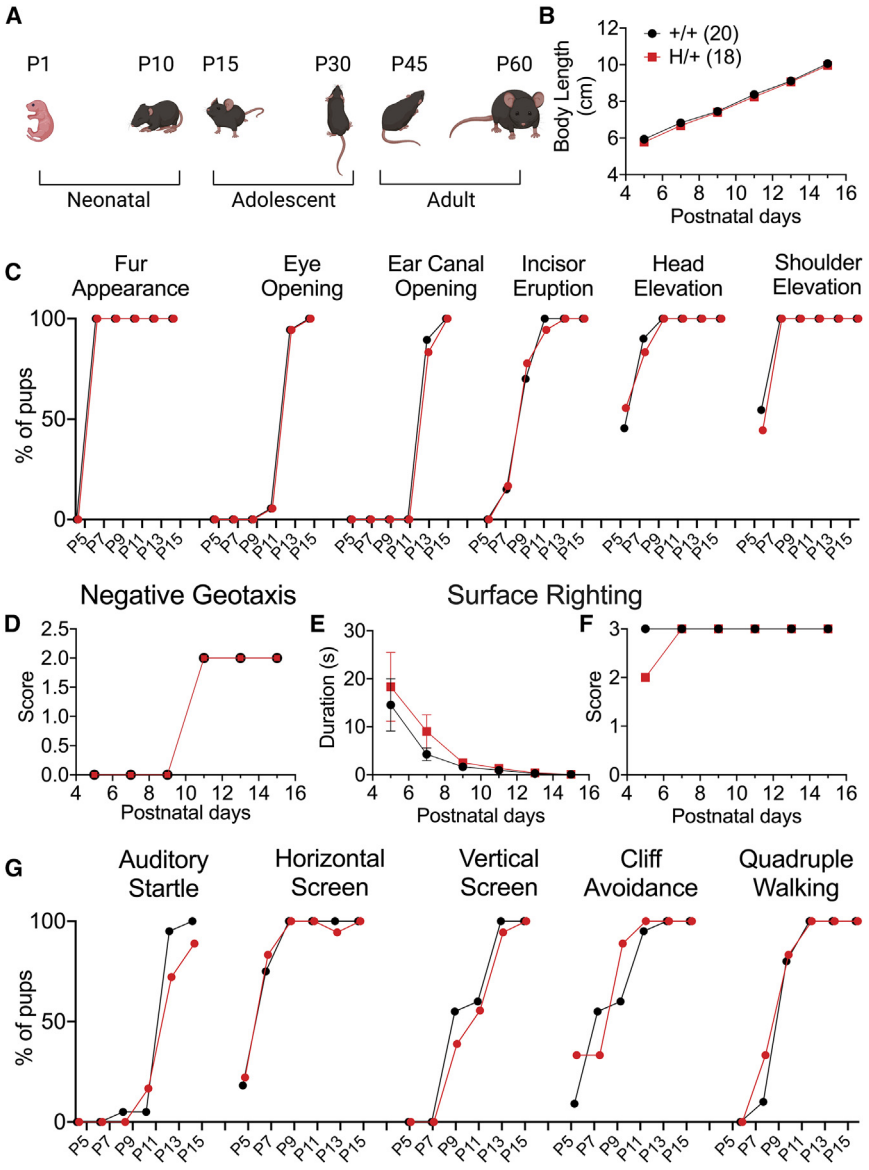


**Figure 2. H/+ mice exhibit normal early physical development and postnatal behavior**

(A) Depiction of mouse developmental stages. Neonatal and young adolescent developmental milestones were evaluated.

(B) Body lengths of +/+ and H/+ mice are identical across the neonatal and early adolescent periods.

(C) Standard mouse developmental and motor behavior benchmarks were achieved at similar time points for both +/+ and H/+ mice.

(D) H/+ mice exhibit normal progression of negative geotaxis (quantified as a geotaxis score).

(E and F) H/+ and +/+ mice succeed in surface righting by P9 as measured by duration to achieve surface righting (E) and surface righting core (F).

(G) H/+ mice show a normal auditory startle reflex and achievement of motor behavioral milestones such as horizontal screen, vertical screen, cliff avoidance, and quadruple walking. See also Table S1. Data shown are mean ± SEM.

Statistical analysis: two-way ANOVA with Šídák's multiple comparisons test (B and D–F). For (B)–(G): +/+ mice, n = 20; H/+ mice, n = 18.

generations, and H/+ mice on a pure C57 background were used for experiments. H/+ mice are viable (Figure 1B), and females are fertile and able to breed until approximately 6 ± 2 months of age. H/+ dams yield 5.6 ± 0.8 pups (mean ± SEM from 10 litters), and wild-type (WT; +/+) and H/+ pups are of normal weight up to/at weaning, while homozygous (H/H) pups are significantly smaller (+/+ vs. H/H, p = 0.0240 via two-way ANOVA with Šídák's multiple comparisons test; Figures 1C and 1D). H/+ mouse body weight at 6 months of age remains normal relative to WT (Figure 1F). H/+ mouse brain size was similar to WT at postnatal day 16 (P16) (Figure 1E) and at age 6 months, relative to age-matched WT littermates (Figures 1G and 1H). There are no differences in body weight or brain weight between +/+ and H/+ mice when males and females are analyzed separately (Figure S2). Histological analysis of cerebellar morphology in both 2- and 6-month-old mouse brains from H/+ mice showed no gross structural abnormality or evidence of cell loss (Figure 1I). Detailed analysis of cerebellar layer thickness showed no Purkinje neuron or granule cell loss in H/+ mice, even at 9 months of age (Figure S3). Spontaneous seizures were observed in H/+ mice starting at/after 4 months of age; we did not observe spontaneous seizures in H/+ mice before 2 months of age. All homozygous H/H mice exhibited reflex- and handling-induced seizures and were deceased prematurely between P16 and P21 (Figure 1B).

## H/+ mice exhibit normal early development

We compared the postnatal behavior and developmental milestones of +/+ and H/+ mice using a standardized observational battery at P5, P7, P9, P11, P13, and P15[27] and observed no differences. There was normal body length progression with time, with no genotype difference (p = 0.1084 via two-way ANOVA) (Figure 2B). There was no difference between +/+ and H/+ mice in timing of fur appearance (P7), shoulder (P7) and head elevation (P9), incisor eruption (P11), eye opening (P13), or ear canal opening (P13) (Figure 2C). H/+ mice also showed normal development of negative geotaxis (Figure 2D). At earlier time points of P5 and P7, a proportion of mice from both +/+ and H/+ groups spent longer than 10 s for surface righting to be elicited, but there was no overall group difference (Figures 2E and 2F). H/+ mice also exhibited a normal auditory startle response (Figure 2G). All neonatal motor behaviors, including horizontal and vertical screen, cliff avoidance, and quadruple walking, were not significantly different between genotypes (Figure 2G).

CellPress
OPEN ACCESS

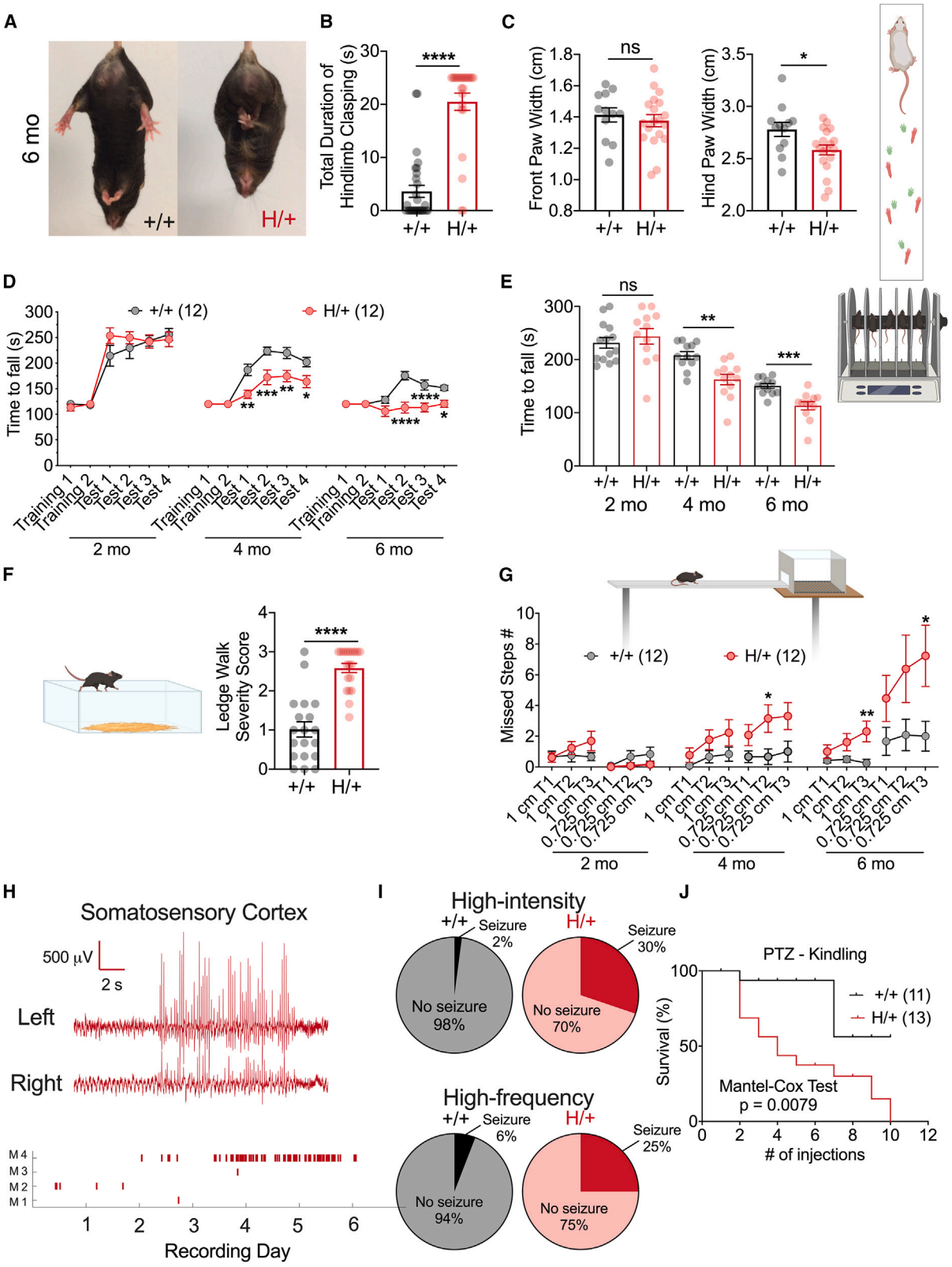


*(legend on next page)*

### The H/+ mouse model phenocopies key features seen in human patients with EPM7

To assess gross motor impairment and ataxia in H/+ mice at later ages, we performed a set of behavioral tests sensitive to cerebellar dysfunction,[28,29] including the tail suspension test (Figures 3A and 3B), paw-print analysis (Figure 3C), accelerating rotarod assay (Figures 3D and 3E), ledge test (Figure 3F), and elevated beam walk test (Figure 3G), on H/+ mice and age-matched +/+ littermate controls across a range of relevant ages. Hindlimb clasping, a commonly used and sensitive indicator of cerebellar ataxia,[30] was prominent upon tail suspension in 6-month-old H/+ mice relative to +/+ (Figure 3B). At 6 months of age, H/+ mice also showed impaired performance on the ledge test with an increased severity score (Figure 3F). H/+ mice exhibited decrease hind paw stance width during assessment of gait via paw-print analysis, consistent with ataxia (Figure 3C). After two training sessions at a set speed, mice were tested on the accelerating rotarod, which revealed progressive deficits in performance in H/+ mice relative to +/+ (Figures 3D and 3E). In the elevated beam walk test,[31] H/+ mice made more errors in hind paw placement compared to age-matched +/+ littermates at both 4 and 6 months of age (Figure 3G).

Spontaneous seizures were observed in H/+ mice starting at 4 months of age. H/+ mice, but not +/+ controls, displayed audiogenic seizures at P18–P20 in response to both high-intensity and high-frequency auditory stimuli (Figure 3I), suggesting increased seizure susceptibility at younger ages. H/+ mice also exhibited markedly accelerated pentylenetetrazol (PTZ)-induced kindling on the PTZ seizure threshold test relative to age-matched +/+ littermate controls, initiated at P30 (Figure 3J). We performed continuous video electroencephalogram (EEG) monitoring in a cohort of H/+ mice at 6 months of age and observed spontaneous recurrent seizures in a subset of mice (Figure 3H), which were brief (no longer than 15 s) and characterized by arrest of activity, occasionally accompanied by head nod and/or limb twitch.

Hence, H/+ mice represent a valid and tractable model of EPM7, recapitulating core clinical phenotypes including age-dependent/progressive ataxia and increased seizure susceptibility, with epilepsy in a subset of mice at/after 4 months of age. The major phenotypic differences observed in H/+ mice are present in both male and female mice (Figure S4).

### Progressive impairment of cerebellar granule cell excitability and parallel fiber-to-Purkinje cell synaptic transmission in H/+ mice

We attempted to link the behavioral abnormalities identified in H/+ mice with underlying cellular and circuit dysfunction. Ataxia, hindlimb clasping and impaired performance on the rotarod, ledge test, and elevated beam walk test suggest cerebellar pathology. As Kv3.1 is known to be prominently expressed in cerebellar granule cells (CGCs),[32,33] we performed targeted whole-cell current-clamp recordings from CGCs in H/+, H/H, and age-matched +/+ littermate controls at age P16–P20 and in +/+ and H/+ mice at 2, 4, and 6 months old (Figures 4A and 4B; Tables S2, S3, and S4). We identified abnormal parameters consistent with Kv3 channel dysfunction, including action potential broadening (measured as prolonged AP half-width, in ms; Figure 4C), prolonged duration of the afterhyperpolarization (measured from AP threshold to the depth of the fast afterhyperpolarization [AHP], in ms; Figure 4D), and decreased maximum instantaneous (Figure 4E) and steady-state firing frequency (in Hz; Figure 4F). These abnormalities were more pronounced for H/H than for H/+ mice at P16–P20 (beyond which time all H/H mice were deceased), while such abnormalities persist to later time points in surviving H/+ mice (Figures 4C–4F). In contrast, we found no difference in passive membrane properties (Table S2) other than an isolated difference in rheobase current injection between H/+ and +/+ mice at the 4 month time point.

Kv3.1 is also expressed at parallel fiber synapses,[33,34] and synaptically localized Kv3 is known to regulate spike width at the synaptic terminal, limiting spike-evoked calcium influx to regulate short-term synaptic plasticity.[25] To determine if synaptic transmission at the parallel fiber-to-Purkinje cell synapse was affected in H/+ mice, we recorded evoked excitatory postsynaptic currents (EPSCs) in Purkinje cells in response to extracellular stimulation of parallel fibers (Figures 4G–4L). We found a

**Figure 3. H/+ mice exhibit age-related motor dysfunction and seizure susceptibility**

(A and B) At 6 months of age, H/+ mice exhibit a severe hindlimb clasping phenotype (A) with longer bouts of clasping (B). +/+ mice, n = 29; H/+ mice, n = 24.

(C) H/+ mice at 6 months old also show reduced hind paw stance width as assessed by paw-print analysis of gait. +/+ mice, n = 12; H/+ mice, n = 19.

(D and E) H/+ mice show impaired performance on the rotarod. H/+ mice exhibit increasingly impaired performance on the accelerating Rotarod relative to +/+ at both 4 and 6 month time points. +/+ mice, n = 12; H/+ mice, n = 12. As described in the method details, each mouse was tested on the rotarod in 4 repeated test sessions (D), and the average measure obtained across the 4 sessions is plotted (E).

(F) At age 6 months, approximately 30% H/+ mice (compared to 5% +/+ mice) cannot traverse the ledge of the home cage during the ledge test. Among mice that are able to complete the traversal, H/+ mice show a higher severity score. +/+ mice, n = 19; H/+ mice, n = 20.

(G) H/+ mice exhibit impaired performance on the elevated beam walking test. H/+ mice made progressively more hindlimb foot faults while traversing a beam of two different diameters with increasing age relative to performance of age-matched +/+ littermate controls (G). Shown is summary data indicating that H/+ mice exhibited progressively more foot faults with age. +/+ mice, n = 12; H/+ mice, n = 12. Each mouse walked on the elevated beam 3 times.

(H) Spontaneous seizures in H/+ mice. Shown on the top is a representative example of an EEG trace from a 6-month-old H/+ mouse demonstrating a seizure event. On the bottom are the summary data indicating the number of seizure events occurring each day during a 7 day recording period of four H/+ mice. Dataset includes two males and two females.

(I) H/+ mice at P16–P21 were susceptible to audiogenic seizure, either with a high-intensity (top; siren; +/+ mice, n = 48; H/+ mice, n = 53) or a high-frequency stimulus (bottom; sonicator; +/+ mice, n = 17; H/+ mice, n = 20).

(J) H/+ mice are more sensitive to PTZ-induced kindling relative to their +/+ siblings as demonstrated by the PTZ seizure threshold test (see STAR Methods). +/+ mice, n = 11; H/+ mice, n = 13. See also Figure S4. Data are presented as mean ± SEM.

Statistical analyses: unpaired Student's t test (B, C, E, and F), two-way ANOVA with Šídák's multiple comparisons test (D and G), Mantel-Cox test (J), and Fisher's test, intensity: p = 0.0001, frequency: p = 0.1886 (I). *p < 0.05, **p < 0.01, ***p < 0.001, and ****p < 0.0001. Exact p values can be found in Table S1.

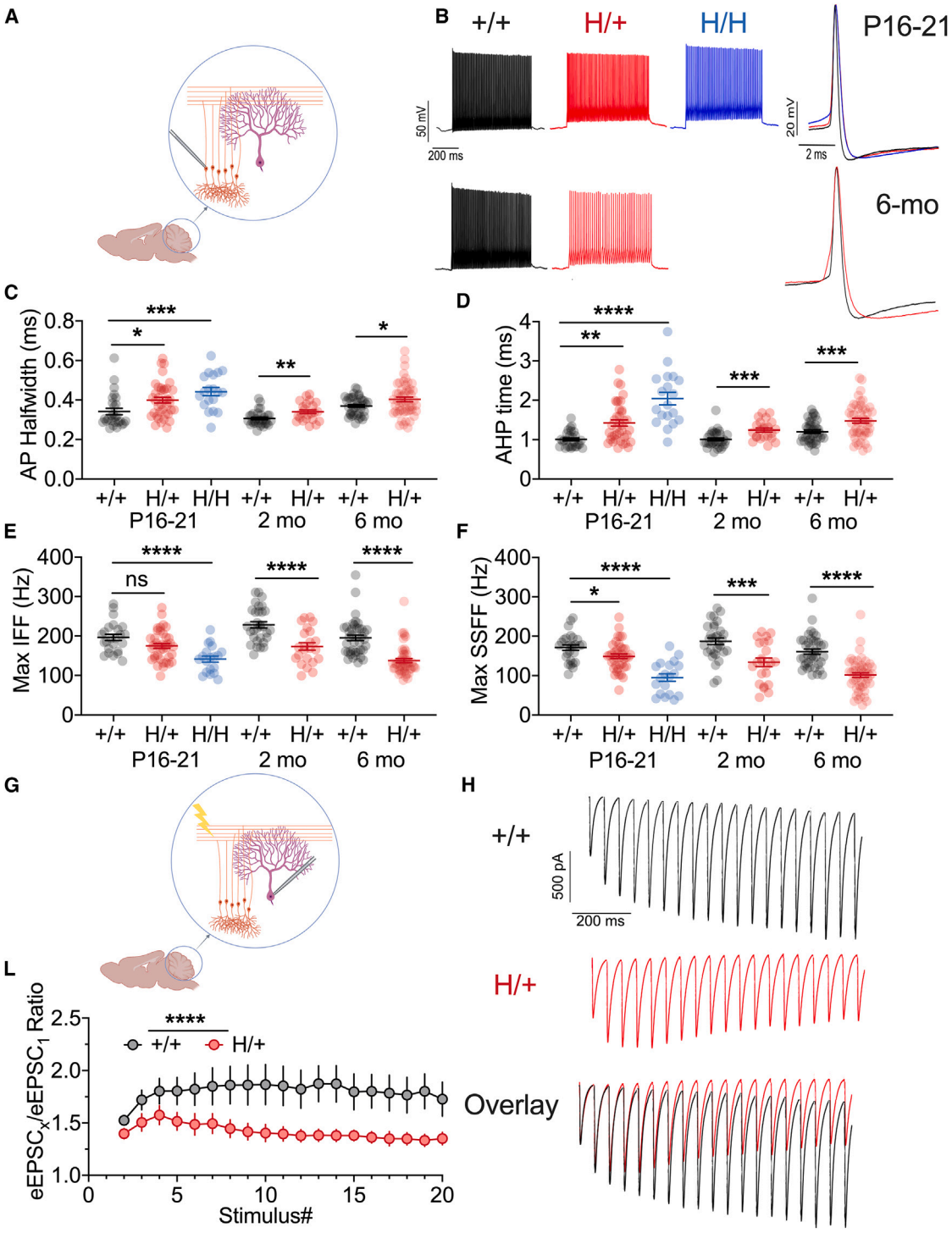


**Figure 4. Impaired cerebellar granule cell function in H/+ mice**

(A) Cerebellar granule cells (CGCs) exhibit age-related impairments of intrinsic excitability in H/+ and H/H mice relative to +/+ mice.

(B) Representative voltage traces from +/+ (black), H/+ (red), and H/H (blue) CGCs obtained via whole-cell patch-clamp recordings in acute brain slice prepared from mice age P16–P21 (top) and at 6 months of age (bottom). Shown on the left is the firing pattern at five-times rheobase current injection. Overlay of a single action potential (right) illustrates spike broadening in H/+ and H/H mice.

(C–F) Summary data for CGC properties dependent upon Kv3 function, including action potential half-width (C) and AHP duration (D), as well as maximum instantaneous (E) and steady-state firing frequency (F) in response to a 600 ms depolarizing pulse. Abnormalities are apparent at P16–P21 between +/+ and H/H

*(legend continued on next page)*

marked alteration of short-term synaptic plasticity—with less facilitation—at parallel fiber synapses in H/+ mice relative to WT controls at 6 months of age (Figures 4G–4L): the ratio of $EPSC_5/EPSC_1$ was 1.51 ± 0.09 in H/+ mice (n = 18) vs. 1.80 ± 0.13 in WT (n = 15, p = 0.08), while the ratio of $EPSC_{10}/EPSC_1$ was 1.40 ± 0.09 in H/+ mice vs. 1.87 ± 0.19 in WT (p = 0.006 vs. H/+ mice).

## Abnormal excitability of neocortical GABAergic INs and impaired IN-to-principal cell synaptic transmission in H/+ mice

We next considered the cellular/circuit basis of the increased susceptibility to seizure observed in H/+ mice. In the neocortex and hippocampus, Kv3.1 is known to be specifically expressed in PV-INs, with the most prominent expression of Kv3.1 in the neocortex in PV-INs in layers 2/3 and 4.[18] We performed recordings of PV-INs in layers 2–4 of the primary somatosensory (“barrel”) neocortex of *Kcnc1*.PV-Cre.tdT triple-transgenic mice and age-matched WT.PV-Cre.tdT littermate controls and quantified a range of standard measures including passive membrane properties, individual action potentials, and repetitive firing (Tables S5–S7). PV-INs in H/H mice at P16–P21 displayed abnormalities specifically in features known to depend on Kv3 channel function (Figures 5A–5F), including action potential half-width (Figure 5C), duration of the fast, deep AHP (Figure 5D), and maximal instantaneous (Figure 5E) and steady-state firing frequencies (Figure 5F). Impairment of PV-INs was progressive in H/+ mice (Figures 5C–5F) and persisted at 6 months (Figures 5C–5F). However, immunohistochemistry showed no loss of PV-INs in the sensorimotor neocortex in H/+ mice aged 6 months or older (Figure S5), suggesting that neocortical circuit hyperexcitability is due to electrophysiological dysfunction of PV-INs rather than selective PV-IN cell death.

Kv3.1 is also prominently expressed at PV-IN synapses.[18,25,32] To assess the impact of the Kv3.1-Arg320His variant on PV-IN synaptic transmission, we performed multiple whole-cell patch-clamp recordings from identified tdTomato-positive PV-INs as well as target excitatory principal cells in layers 2–4 of the primary somatosensory neocortex, recording unitary evoked inhibitory postsynaptic currents (IPSCs) in principle cells (in voltage clamp) in response to action potentials in presynaptic PV-INs (generated in current clamp; Figures 5G–5J). In acute brain slices prepared from WT, H/+, and H/H mice aged P16–P21, IPSCs were recorded in postsynaptic principal cells using pipettes filled with an internal solution containing high (63 mM) chloride (Cl) such that $E_{Cl} = -17$ mV and GABA-mediated inhibitory postsynaptic potentials (IPSPs) were recorded as depolarizations from resting membrane potential, while IPSCs were recorded as large inward currents in voltage clamp at a holding potential of −80 mV. We stimulated presynaptic PV-INs to discharge trains of repetitive action potentials at various frequencies (20, 40, and 120 Hz) and identified enhanced short-term synaptic depression in H/+ and H/H mice relative to +/+ (Figure 5J). However, IPSC amplitude (Figure S6A) and latency (Figure S6B) were the same between H/+ and +/+ mice. The failure rates of the first and fifth IPSCs were not significantly different between genotypes (Figures S6C–S6H).

## AUT00206 is a specific positive modulator of Kv3 channels, including those containing the p.Arg320His variant subunit

Prior work in *Xenopus* oocytes showed that the human *KCNC1*-p.Arg320His variant exerts loss of function via presumptive dominant-negative action on tetrameric Kv3.1-containing K+ channels (Figure S9).[2] We confirmed in a heterologous mammalian cell system that Kv3.1-Arg320His produces a loss of channel function (Figure S7). Currents were recorded from HEK293T cells expressing Kv3.1-WT (Figures S7A–S7C), Kv3.1-Arg320His (Figures S7D–S7F), or WT + Arg320His (Figures 6A–6C) in a 1:1 ratio (the latter so as to better approximate the heterozygous state of the variant in patients with EPM7). Kv3.1-Arg320His leads to a ∼60% reduction in peak current density compared to cells expressing WT channel subunits: current density was 508 ± 155 pA/pF at +40 mV for Kv3.1-Arg320His (n = 10) vs. 1,241 ± 88 pA/pF for WT (n = 15; p = 0.0002; unpaired Student’s t test). Cells co-expressing WT + Arg320His-Kv3.1 channels also led to a significant (44%) reduction in peak current density of 702 ± 175 pA/pF (n = 10; p = 0.006 vs. WT; unpaired Student’s t test), suggesting that Kv3.1-Arg320His channel subunits could lead to suppression of Kv3 current in mammalian cells. Given these findings, we postulated that increasing Kv3 activity may represent a viable therapeutic approach toward ameliorating the cellular, circuit, and behavioral abnormalities identified in H/+ mice.

We then tested the effect of a Kv3 positive modulator, AUT00206 (Figure S1), on the function of Kv3 channels expressing Kv3.1-WT or Arg320His subunits. We found that 10 μM AUT00206 produced a small increase in conductance and a leftward shift in the voltage dependence of activation curve for human *KCNC1*-p.Arg320His expressed in *Xenopus* oocytes (Figure S9). AUT00206 also produced a left shift in the voltage dependence of activation curve of Kv3.1-WT expressed in HEK293T cells: the $V_{1/2}$ of activation was +13.1 ± 0.9 mV for Kv3.1-WT + vehicle (n = 15) vs. −1.1 ± 1.9 mV after application of 30 μM AUT00206 (n = 14; p < 0.0001; paired t test), and the $V_{1/2}$ of activation was 9.2 ± 1.4 mV for Kv3.1-Arg320His + vehicle

mice and between +/+ and H/+ mice at the 2 and 6 month time points. P16–P21: H/H mice, n = 19; H/+ mice, n = 39; +/+ mice, n = 27; 2 months: +/+ mice, n = 31; H/+ mice, n = 23; 6 months: +/+ mice, n = 40; H/+ mice, n = 50.

(G–L) Impaired short-term synaptic plasticity at the parallel fiber synapse in H/+ mice. (G) Stimulation of the parallel fibers produces evoked excitatory postsynaptic currents (EPSCs) in Purkinje neurons, the output neurons of the cerebellum. (H) Representative traces of evoked EPSCs in response to a 20 pulse train at 20 Hz in a brain slice prepared from 6-month-old +/+ (black) and H/+ (red) mice, with overlay. (I) Synaptic ratio is calculated as the amplitude of evoked EPSC $(eEPSC)_X$ relative to the first eEPSC ($eEPSC_1$). Data are mean ± SEM. +/+ mice, n = 15; H/+ mice, n = 18. See also Tables S2–S4, S9, and S10.

Statistical analyses: P16–P21, one-way ANOVA with Šídák’s multiple comparison (C–F); 2 and 6 months of age: unpaired Student’s t test (C and D), Mann-Whitney test (E and F), or two-way ANOVA with Šídák’s multiple comparisons test (I). *p < 0.05, **p < 0.01, ***p < 0.001, and ****p < 0.0001. Exact p values and experimental n can be found in Table S1.

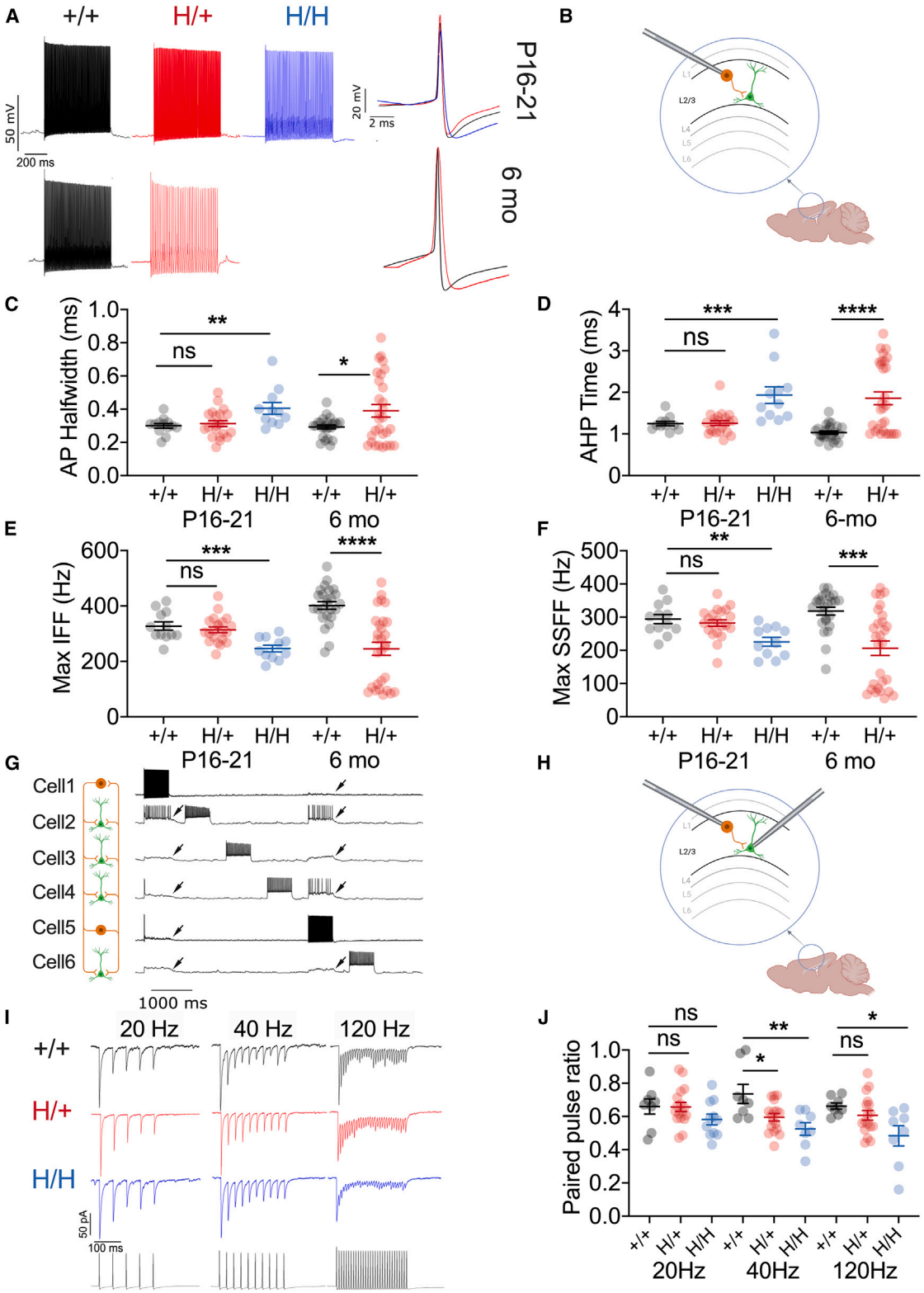


**Figure 5. Impaired excitability of neocortical PV-positive GABAergic interneurons in H/+ mice**

(A) PV-positive GABAergic interneurons (PV-INs) show age-related abnormalities of intrinsic excitability. Shown are representative voltage traces from PV-INs in +/+ (black), H/+ (red), and H/H (blue) mice at five-times rheobase current injection in acute brain slices from mice aged P16–P21 and 6 months old.

*(legend continued on next page)*

(n = 13) vs. −2.4 ± 1.4 mV after application of 30 μM AUT00206 (n = 12; p < 0.0001; unpaired Student's t test) (Figure S7). When WT and Kv3.1-Arg320His were co-expressed in a 1:1 ratio, we found that $V_{1/2}$ was +13.6 ± 1.6 mV for WT + ArgR320His (vehicle; n = 13) vs. −1.3 ± 3.8 mV after application of 30 μM AUT00206 (n = 9; p = 0.0006; paired t test; Figure 6C). At −10 mV, peak current increased an average of 2.5-fold with the application of 30 μM AUT00206, from 1,955 ± 356 pA/pF in vehicle (DMSO) to 5,245 ± 1,297 pA/pF with AUT00206 (n = 9; p = 0.0112 via paired Student's t test; Figure 6B). Such data suggest that Kv3.1-p.Arg320His leads to a partial loss of function in mammalian cells and that the Kv3 current at physiologically relevant voltages at/around the peak of the fast-spiking PV-IN action potential can be augmented by AUT00206.

### AUT00206 enhances repetitive firing of CGCs and neocortex PV-positive INs from H/+ mice and improves motor function *in vivo*

Data presented thus far suggest that identified behavioral deficits in H/+ mice, including ataxia and propensity to seizure, may be linked at least in part to dysfunction of Kv3.1-expressing neurons in the cerebellum and neocortex, secondary to decreased Kv3 current due to loss-of-function Kv3.1-Arg320His subunits. Since the Kv3 current mediated by WT and variant Kv3.1-Arg320His can be augmented with the Kv3-specific positive modulator AUT00206, we next tested whether AUT00206 improves identified impairments in the cellular excitability of Kv3.1-expressing CGCs in H/+ mice. We performed whole-cell recording of CGCs in acute brain slices from 6-month-old H/+ and age-matched WT control mice and found that bath application of 100 μM AUT00206 enhances repetitive firing of CGCs in both WT and H/+ mice (Figures 6D and 6E), while vehicle control has no effect (Figures S8A and S8B). Bath application of AUT00206 produced no effect on the firing properties of non-Kv3-expressing neocortical pyramidal cells (Figures S8C and S8D). We also found that 100 μM AUT00206 enhanced spike fidelity (the time-locking of stimulus to action potential output) and following frequency (the proportion of stimuli that succesfully generate action potentials) of PV-INs[35] in 6-month-old H/+ mice in response to high-frequency stimulation (Figures 6F and 6G).

We then tested the effect of AUT00206 *in vivo*. Doses were chosen based on previous studies that have shown central effects of AUT00206 in a range of rodent models following systemic administration.[36,37] Pharmacokinetic data for AUT00206 in H/+ mice were not available; however, the half-life of AUT00206 following intraperitoneal (i.p.) dosing in C57BL/6J mice is 2–3 h (Autifony Therapeutics). Furthermore, the compound is well tolerated over a range of doses in preclinical models and in human studies, having completed long-term toxicity studies in animals and assessment of safety and tolerability studies in human subjects. We assessed the impact of AUT00206 on the performance of 6-month-old H/+ and age-matched WT mice on the rotarod and ledge tests. We found that a single i.p. injection of AUT00206 at 30 mg/kg delivered 45–60 min prior to testing enhanced performance on the rotarod (Figure S10A) and eliminated the difference between WT and H/+ mice (Figure 6H; WT vehicle vs. H/+ vehicle; p = 0.0151; WT AUT00206 vs. H/+ AUT00206, p = 0.9326; via unpaired Student's t test). A single i.p. injection of AUT00206 at 30 mg/kg also reduces the severity score of H/+ mice performance on the ledge test (Figure S10B) and eliminates the difference between WT and H/+ mice (Figure 6I).

To assess the effect of AUT00206 on the seizure phenotype of H/+ mice, we first tested the impact of AUT00206 on seizure susceptibility in the PTZ seizure threshold test. Acute administration of AUT00206 (30 mg/kg) at 45 min prior to each PTZ dose led to a marked improvement in survival of H/+ mice, such that the proportion of mice surviving or non-kindled at the experimental endpoint was not different between treated WT and H/+ mice (Figure 6J; WT vehicle vs. H/+ vehicle, p < 0.0001; WT AUT00206 vs. H/+ AUT00206, p = 0.0986, via Mantel-Cox test). Subgroup analysis revealed no effect of sex on the efficacy of AUT00206 (Figure S11). We then performed continuous video EEG on a cohort of 6-month-old H/+ mice and tested the response to AUT00206. Overall seizure frequency among 19 H/+ mice was 4.4 ± 2.4 seizures/day. Approximately one-third of 6-month-old H/+ mice exhibited two or more spontaneous seizures during a 3 day monitoring period (Figure 6K), and we selected these mice for a subsequent trial of AUT00206. We found that AUT00206 injected at 30 mg/kg i.p. for 5 consecutive days led to a marked reduction in seizure frequency (Figure 6L), with reduction observed in all 6 mice and a mean decrease from 13.9 ± 6.4 to 4.0 ± 2.1 per day (p = 0.1441 via paired t test). 4 out of 6 mice exhibited no seizures for each 3 h period postinjection across 5 days. 48 h after the last injection of AUT00206 (AUT6; washout), 1 out of 6 mice was deceased, while 5 of 5 remaining mice reverted to a pretreatment seizure frequency of 7.2 ± 2.3 seizures/day.

## DISCUSSION

EPMs are a group of ultrarare but devastating neurological disorders, characterized by onset and progression of myoclonus

(B) PV-INs were recorded in layers 2–4 of primary somatosensory neocortex.
(C–F) Summary data for electrophysiological properties dependent upon Kv3 function, including action potential (AP) half-width (C), AHP time (D), and maximum instantaneous (E) and steady-state firing frequency (F). P16–P21: H/+ mice, n = 11; H/+ mice, n = 22; +/+ mice, n = 25; 6 months: H/+ mice, n = 29; +/+ mice, n = 25. See Figure S4 for additional parameters.
(G–J) Both H/+ and H/H showed impaired PV-IN:principal cell synaptic transmission at P16–P21. (G) Representative voltage traces obtained via multiple whole-cell current-clamp recording of two PV-INs (cells 1 and 5) and 4 pyramidal cells (cells 2, 3, 4, and 6). (H) Multiple simultaneous whole-cell recordings from identified tdTomato-positive PV-INs as well as principal cells in layers 2–4 of the primary somatosensory neocortex. (I) Representative examples of evoked unitary inhibitory postsynaptic currents (uIPSCs) at 20, 40, and 120 Hz from acute brain slices prepared from +/+, H/+, and H/H mice at P16–P21. (J) Paired-pulse ratio is significantly lower in both H/+ and H/H mice relative to +/+ mice at 40 and 120 Hz. H/H mice, n = 8; H/+ mice, n = 17; +/+ mice, n = 11. See also Tables S1 and S6–S10. Data are presented as mean ± SEM.
Statistical analyses: one-way ANOVA with Šídák's multiple comparison test at P16–P21 (C–F and J) and unpaired Student's t test or Mann-Whitney test at 6 months of age (C–F). *p < 0.05, **p < 0.01, ***p < 0.001, and ****p < 0.001. Exact p values and experimental n can be found in Table S1.

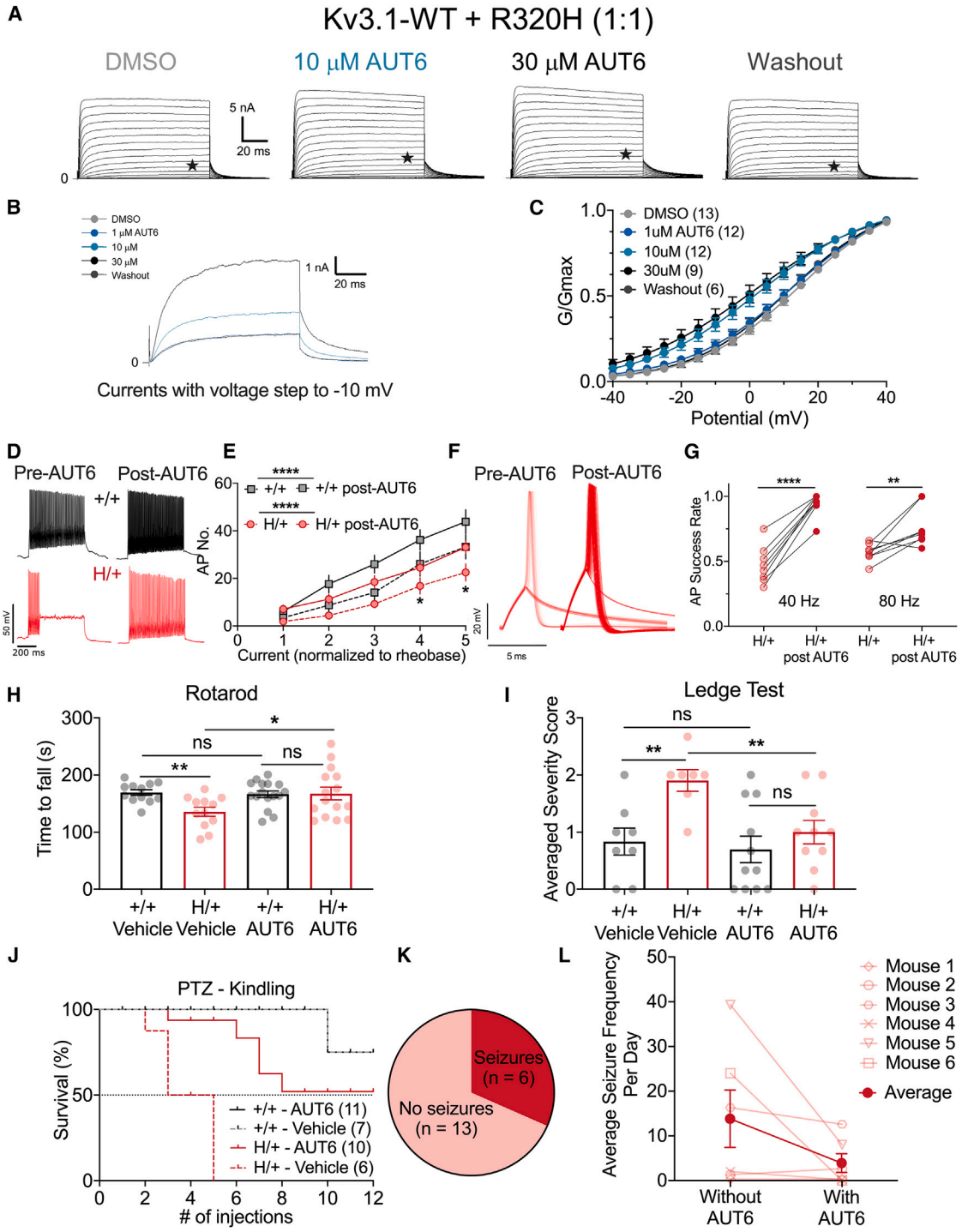


**Figure 6. AUT00206 modulates Kv3 current, enhances CGC excitability, and improves motor function and seizure susceptibility of H/+ mice**

(A–C) HEK293T cells co-transfected with Kv3.1-WT and Kv3.1-Arg320His variant at a 1:1 ratio. Shown in (A) are families of currents generated in response to voltage steps from −40 to +40 mV in increments of 5 mV from a holding potential of −80 mV. (B) Overlaid currents generated in response to voltage steps to −10 mV (indicated by a star [★] in A) under control conditions (light blue), after application of 10 and 30 μM AUT00206 (dark blue), and after washout (black; overlaid with control trace). AUT00206 (AUT6) produces a leftward shift in the conductance-voltage (*G-V*) plot and increased current/conductance at relevant voltages (C). DMSO, n = 13; 10 μM, n = 12; 30 μM, n = 12; 100 μM, n = 9; washout, n = 6.

(D) Representative traces of CGC firing from 6-month-old mice before/after bath application of 100 μM AUT6.

(E) Current-frequency (*I-f*) curves show increased excitability of CGCs from both +/+ and H/+ mice with application of AUT6. +/+ mice, n = 20; H/+ mice, n = 20.

*(legend continued on next page)*

and epilepsy, often accompanied by tremor and ataxia, in previously healthy children, adolescents, and young adults, with relentless neurological deterioration leading to loss of ambulation and functional limb use, severe disability, and, in some cases, early death. The gene variants associated with many types of EPM have been identified. Yet, even when a specific genetic diagnosis can be made, EPMs are largely intractable to currently available treatments, which have limited symptomatic benefit. Thus, further studies into disease pathomechanisms are urgently required to drive the development of novel treatments and, ideally, targeted therapeutic approaches that address the underlying molecular defect or resulting cellular or circuit dysfunction. Such approaches may offer greater potential for treatment efficacy and, if administered early enough in the disease course, could modify or even prevent disease progression.

## Disease mechanisms of EPM7

EPM7 is due to the recurrent variant *KCNC1* c.959G>A (p.Arg320His), which—unique among all EPMs—encodes an ion channel pore-forming subunit. The recent cryoelectron microscopy (cryo-EM) structure of human Kv3.1a provides insight into the molecular mechanism whereby this might occur, suggesting that the positively charged arginine at position 320 forms an electrostatic interaction with Asp282 in S3 and participates in a cation-$\pi$ interaction with the aromatic ring of Phe256 in S2, which may be disrupted via mutation to histidine to impact gating.[38] EPM7 is characterized by the combination of epilepsy and progressive action and reflex myoclonus along with tremor and ataxia, with neurological decline leading to loss of ambulation and functional limb use. Most or all patients with EPM7 have epilepsy, although seizure frequency is low (particularly during the chronic/plateau phase of the disorder in adults) and is not considered the most debilitating aspect of the disorder; however, patients typically remain on a chronic regimen of conventional anti-seizure medications in an attempt to manage myoclonus. Prior work has shown the *KCNC1*-p.Arg320His variant causes a near-complete loss of function in *Xenopus* oocytes (see Figures S9A–S9C) and a putative dominant-negative effect when co-expressed with WT Kv3.1 subunits.[2,3] Our data confirm the general loss-of-function effect of the Kv3.1-Arg320His variant but suggest only a partial loss. The basis for this discrepancy is unknown but may relate to differences in expression of Kv3-interacting proteins between heterologous cell systems. However, it is clear from our studies that even a partial loss of function with dominant-negative action is sufficient to significantly alter the firing properties of native Kv3.1-expressing neurons, such as CGCs and neocortical PV-INs.

## Targeted modulation of Kv3 for treatment of EPM7

All prior studies of the *KCNC1*-p.Arg320His variant have been undertaken *in vitro* in heterologous cells or primary neurons in culture via overexpression of Kv3.1.[39] Hence, we generated a H/+ mouse model via CRISPR-Cas9, which we show to recapitulate the core clinical features of EPM7, including progressive ataxia and susceptibility to seizure. H/+ mice do not exhibit a severe epilepsy phenotype, similar to human patients; however, H/+ mice do exhibit audiogenic seizures at P16–P21, a lowered threshold for PTZ kindling, handling-induced seizures starting at/around 4 months of age observed during standard colony maintenance (data not shown), and spontaneous seizures in at least a subset of mice at/beyond 6 months of age. We explored the cellular- and circuit-level basis for this neurological dysfunction and identified impaired firing as well as altered properties of individual action potentials and of synaptic transmission by Kv3.1-expressing neurons in relevant brain areas linked to EPM7 pathology in H/+ mice, including neocortical PV-INs and CGCs. Prior work showed that the small-molecule Kv3 activator RE01 (AUT1, Autifony Therapeutics) increases Kv3 currents mediated by both WT Kv3.1 and Kv3.1-Arg320His.[40] We tested a more specific Kv3 channel modulator, AUT00206, which we show increases activity of K+ channels containing WT and variant Kv3.1-Arg320His in heterologous systems, improves cellular dysfunction of Kv3.1-expressing CGCs in H/+ mice, and ameliorates ataxia, seizure susceptibility, and epilepsy in H/+ mice *in vivo*. However, the precise mechanism whereby AUT00206 enhances function of Kv3.1-expressing neurons in H/+ mice may not be entirely clear. It should be noted that AUT00206 acts as a potent and specific positive modulator of WT Kv3 channels and increases the firing frequency of WT cerebellar granule neurons in addition to neurons from H/+ mice. We found that the effect of AUT00206 was observed following co-injection in *Xenopus* oocytes and after co-transfection of HEK293T cells with Kv3.1-WT and Kv3.1-Arg320His (Figures 6A–6C, S7D–S7F, and S9F). AUT00206 also enhances currents mediated by K+ channels composed of homomeric WT Kv3.1 subunits. In native neurons, Kv3 channels are tetramers, likely heterotetrameric assemblies of different Kv3 subunits (e.g., Kv3.1–3.4), or, in the case of EPM7, a mixture of WT and variant Kv3.1 subunits, along with other

(F) Representative traces of action potentials of PV-INs in response to repetitive stimulation at 40 Hz before/after bath application of 100 μM AUT6.
(G) Summary plot of PV-IN firing fidelity in response to 40 and 80 Hz repetitive stimulation before and after bath application of 100 μM AUT6. 40 Hz, n = 8; 80 Hz, n = 8.
(H) A single i.p. injection of 30 mg/kg AUT6 improves performance on the rotarod. H/+ mice: vehicle, n = 9; AUT6, n = 15. +/+ mice: vehicle, n = 12; AUT6, n = 16. Each mouse received 4 test sessions on the rotarod. Shown here is the average of the 4 test sessions.
(I) A single i.p. injection of 30 mg/kg AUT6 improves performance on the ledge test. H/+ mice: vehicle, n = 7; AUT6, n = 10. +/+ mice: vehicle, n = 7; AUT6, n = 11.
(J) Acute i.p. injections of 30 mg/kg AUT6 delivered 45–60 min prior to PTZ administration attenuates kindling epileptogenesis in H/+ mice. Note that the two lines, +/+ vehicle (gray) and +/+ AUT6 (black), are completely superimposed. H/+ mice: vehicle, n = 6; AUT6, n = 10. +/+ mice: vehicle, n = 7; AUT6, n = 11.
(K) Continuous video EEG detected baseline spontaneous seizures (2 or more seizures in 72 h) in 6 out of 19 mice.
(L) Summary of average seizure frequency per day during baseline monitoring (vehicle, without AUT6) and drug delivery phase (with AUT6) in the 6 mice with spontaneous seizures. See also Figures S7–S11 and Table S1. Data are mean ± SEM.
Statistical analyses: two-way ANOVA with Šídák's multiple comparisons test (E), paired t test (G and L), unpaired t test (H and I), and Mantel-Cox test (J). *p < 0.05, **p < 0.01, ***p < 0.001, and ****p < 0.001. Exact p values and experimental n can be found in Table S1.

non-Kv3.1 Kv3 subunits. It is probable that native neurons in patients with EPM7 express a diversity of Kv3 channels containing such subunits at different ratios. Thus, we cannot be certain as to whether effects of AUT00206 in H/+ mice are predominantly due to action on Kv3 channels containing Kv3.1-Arg320His subunits and/or on WT channels.

Both CGCs and neocortical PV-INs from H/+ mice showed impaired firing properties, consistent with decreased net Kv3.1 current; however, Kv3.1-expressing neurons in other brain regions were unaffected, at least at P16–P21. Specifically, we recorded Kv3.1-expressing PV-INs in the hippocampus, reticular thalamic nucleus, auditory neocortex, and inferior colliculus in H/+ mice and found no significant genotype-related differences in these brain areas (Tables S8–S10). The basis of any region-specific dysfunction is also unclear but may relate to the differential co-expression of other Kv3 subfamily members[41] and/or regional differences in compensatory mechanisms. Future work will evaluate these brain areas and cell types—including Kv3-expressing cerebellar molecular layer INs not included in this study—including at later time points, and it is predicated that, for example, PV-INs in the hippocampus will likely exhibit similar pathology if examined at later time points. It is of interest to note that the phenotype of H/+ mice is more severe than that seen in *Kcnc1*$^{-/-}$ (Kv3.1-knockout) mice,[42] suggesting that a seemingly more subtle missense variant can be more detrimental than deletion, perhaps via dominant action on heterotetrameric channels or via "escape" of compensation. For example, Kv3.3-knockout mice have no obvious motor abnormalities, while Kv3.1/Kv3.3-double-knockout mice have marked tremor and severe ataxia;[43] Kv3.1 and Kv3.3 channels appear to reciprocally compensate for one another in constitutive single-gene-knockout mice.[44]

### Limitations of the study

While we identified a cellular and circuit basis of dysfunction in a preclinical experimental mouse model of EPM7, the mechanism of progression remains unknown. Cellular dysfunction (evident by P16–P21) appears to lead to the appearance of behavioral deficits (at age 2–4 months) and is consistent with the known developmental expression pattern of Kv3.1 in mouse, where Kv3.1 protein does not appear until P10 or later. However, we did not observe any difference in brain size or reduction in the size of the cerebellum, thickness of the layers of the cerebellar cortex, or density of Purkinje cells in the cerebellum, nor did we find reduction of neocortical PV-IN cell numbers. Future work may test whether more prolonged administration of AUT00206 or modulation of Kv3.1-expressing fast-spiking neurons could be neuroprotective or preventative in H/+ mice, particularly if administered from an early age.

### Conclusion

The H/+ mouse model recapitulates the core clinical phenotype, and is a valuable tool for the study, of EPM7. Kv3.1-expressing neurons in the neocortex and cerebellum exhibit specific impairments consistent with decreased Kv3 function. A Kv3 positive modulator, AUT00206, increases Kv3 channel open probability and thus directly counteracts the impact of the Arg320His variant, leading to recovery of fast spiking in Kv3.1-expressing neurons in H/+ mice. At a behavioral level, these effects of AUT00206 translate to improvement of cerebellar dysfunction and a reduction in the propensity of H/+ mice to seizure *in vivo.* Such results suggest the therapeutic potential of Kv3 positive modulators for the treatment of EPM7 and potentially other forms of EPM as well as other Kv3 ion channelopathies. A clinical trial evaluating the effects of a related Kv3 positive modulator, AUT00201, in patients with EPM7 is currently underway (ClinicalTrials.gov: NCT05873062).

## STAR★METHODS

Detailed methods are provided in the online version of this paper and include the following:

- KEY RESOURCES TABLE
- RESOURCE AVAILABILITY
  - Lead contact
  - Materials availability
  - Data and code availability
- EXPERIMENTAL MODEL AND SUBJECT DETAILS
  - Experimental animals
  - Pharmacology
- METHOD DETAILS
  - Behavioral assays of motor function
  - Pentylenetetrazol (PTZ) seizure threshold test
  - Audiogenic seizures
  - EEG recordings
  - Cell culture and transfection
  - Voltage-clamp recording of ionic currents
  - Acute brain slice preparation
  - Electrophysiological recordings in acute brain slice
  - Immunohistochemistry
  - Data analysis
- QUANTIFICATION AND STATISTICAL ANALYSIS

### SUPPLEMENTAL INFORMATION

Supplemental information can be found online at https://doi.org/10.1016/j.xcrm.2023.101389.

### ACKNOWLEDGMENTS

We thank Eric D. Marsh for assistance with video EEG and Phillipe Isope for valuable suggestions on experimental design. This work was funded by a Postdoctoral Fellowship Award from the National Ataxia Foundation (H.F.), NIH NINDS R01 NS122887 (E.M.G.), a Pilot Grant from The Children's Hospital of Philadelphia Intellectual and Developmental Disabilities Research Center (to E.M.G.; MPI, Eric Marsh and Robert Schultz) via NIH NINDS P50 HD105354, a grant from Autifony Therapeutics, Ltd. (E.M.G.), and by generous donations from Team B and the Lauren Arena Fund for MEAK (E.M.G.).

### AUTHOR CONTRIBUTIONS

H.F. conceived of and performed the investigations and formal analysis and wrote, reviewed, and edited the manuscript. J.C., K.K., M.F.-M., E.R.W., C.K., E.H., E.L., D.L., L.A., and Q.L. performed investigations and formal analysis. X.Z. was involved in project administration. A.S. performed formal data analysis. M.C. was involved in project administration and in the review

and editing of the manuscript. M.J.G. and C.H.L. were involved in project administration and review and editing of the manuscript and provided resources (AUT00206). N.A. performed formal analysis and contributed to project administration. E.M.G. was involved in the conceptualization of the research, investigation, and formal analysis, data curation, writing, review, and editing of the manuscript, supervision, project administration, and funding acquisition.

## DECLARATION OF INTERESTS

M.J.G. and C.H.L. are employees and shareholders of Autifony Therapeutics, Ltd.

Received: February 9, 2023
Revised: November 9, 2023
Accepted: December 20, 2023
Published: January 23, 2024

## REFERENCES

1. Nascimento, F.A., and Andrade, D.M. (2016). Myoclonus epilepsy and ataxia due to potassium channel mutation (MEAK) is caused by heterozygous KCNC1 mutations. Epileptic Disord. *18*, 135–138.
2. Muona, M., Berkovic, S.F., Dibbens, L.M., Oliver, K.L., Maljevic, S., Bayly, M.A., Joensuu, T., Canafoglia, L., Franceschetti, S., Michelucci, R., et al. (2015). A recurrent de novo mutation in KCNC1 causes progressive myoclonus epilepsy. Nat. Genet. *47*, 39–46.
3. Oliver, K.L., Franceschetti, S., Milligan, C.J., Muona, M., Mandelstam, S.A., Canafoglia, L., Boguszewska-Chachulska, A.M., Korczyn, A.D., Bisulli, F., Di Bonaventura, C., et al. (2017). Myoclonus epilepsy and ataxia due to KCNC1 mutation: Analysis of 20 cases and K(+) channel properties. Ann. Neurol. *81*, 677–689.
4. Kälviäinen, R. (2015). Progressive Myoclonus Epilepsies. Semin. Neurol. *35*, 293–299.
5. Orsini, A., Valetto, A., Bertini, V., Esposito, M., Carli, N., Minassian, B.A., Bonuccelli, A., Peroni, D., Michelucci, R., and Striano, P. (2019). The best evidence for progressive myoclonic epilepsy: A pathway to precision therapy. Seizure *71*, 247–257.
6. Holmes, G.L. (2020). Drug Treatment of Progressive Myoclonic Epilepsy. Paediatr. Drugs *22*, 149–164.
7. Ferlazzo, E., Trenite, D.K.N., Haan, G.J.d., Felix Nitschke, F., Ahonen, S., Gasparini, S., and Minassian, B.A. (2017). Update on Pharmacological Treatment of Progressive Myoclonus Epilepsies. Curr. Pharm. Des. *23*, 5662–5666.
8. Goldstein, S.A.N., Bayliss, D.A., Kim, D., Lesage, F., Plant, L.D., and Rajan, S. (2005). International Union of Pharmacology. LV. Nomenclature and molecular relationships of two-P potassium channels. Pharmacol. Rev. *57*, 527–540.
9. Coetzee, W.A., Amarillo, Y., Chiu, J., Chow, A., Lau, D., McCormack, T., Moreno, H., Nadal, M.S., Ozaita, A., Pountney, D., et al. (1999). Molecular diversity of K+ channels. Ann. N. Y. Acad. Sci. *868*, 233–285.
10. Spillane, J., Kullmann, D.M., and Hanna, M.G. (2016). Genetic neurological channelopathies: molecular genetics and clinical phenotypes. J. Neurol. Neurosurg. Psychiatry *87*, 37–48.
11. Brenner, R., and Wilcox, K.S. (2012). Potassium Channelopathies of Epilepsy. In Jasper's Basic Mechanisms of the Epilepsies, J.L. Noebels, M. Avoli, M.A. Rogawski, R.W. Olsen, and A.V. Delgado-Escueta, eds. (Oxford University Press).
12. Zhang, Y., and Kaczmarek, L.K. (2016). Kv3.3 potassium channels and spinocerebellar ataxia. J. Physiol. *594*, 4677–4684.
13. Kullmann, D.M. (2010). Neurological channelopathies. Annu. Rev. Neurosci. *33*, 151–172.
14. Weiser, M., Vega-Saenz de Miera, E., Kentros, C., Moreno, H., Franzen, L., Hillman, D., Baker, H., and Rudy, B. (1994). Differential expression of Shaw-related K+ channels in the rat central nervous system. J. Neurosci. *14*, 949–972.
15. Rudy, B., Chow, A., Lau, D., Amarillo, Y., Ozaita, A., Saganich, M., Moreno, H., Nadal, M.S., Hernandez-Pineda, R., Hernandez-Cruz, A., et al. (1999). Contributions of Kv3 channels to neuronal excitability. Ann. N. Y. Acad. Sci. *868*, 304–343.
16. Tansey, E.P., Chow, A., Rudy, B., and McBain, C.J. (2002). Developmental expression of potassium-channel subunit Kv3.2 within subpopulations of mouse hippocampal inhibitory interneurons. Hippocampus *12*, 137–148.
17. Rowan, M.J.M., DelCanto, G., Yu, J.J., Kamasawa, N., and Christie, J.M. (2016). Synapse-Level Determination of Action Potential Duration by K(+) Channel Clustering in Axons. Neuron *91*, 370–383.
18. Chow, A., Erisir, A., Farb, C., Nadal, M.S., Ozaita, A., Lau, D., Welker, E., and Rudy, B. (1999). K(+) channel expression distinguishes subpopulations of parvalbumin- and somatostatin-containing neocortical interneurons. J. Neurosci. *19*, 9332–9345.
19. Erisir, A., Lau, D., Rudy, B., and Leonard, C.S. (1999). Function of specific K(+) channels in sustained high-frequency firing of fast-spiking neocortical interneurons. J. Neurophysiol. *82*, 2476–2489.
20. Rudy, B., and McBain, C.J. (2001). Kv3 channels: voltage-gated K+ channels designed for high-frequency repetitive firing. Trends Neurosci. *24*, 517–526.
21. Kaczmarek, L.K., and Zhang, Y. (2017). Kv3 Channels: Enablers of Rapid Firing, Neurotransmitter Release, and Neuronal Endurance. Physiol. Rev. *97*, 1431–1468.
22. Lau, D., Vega-Saenz de Miera, E.C., Contreras, D., Ozaita, A., Harvey, M., Chow, A., Noebels, J.L., Paylor, R., Morgan, J.I., Leonard, C.S., and Rudy, B. (2000). Impaired fast-spiking, suppressed cortical inhibition, and increased susceptibility to seizures in mice lacking Kv3.2 K+ channel proteins. J. Neurosci. *20*, 9071–9085.
23. Lien, C.C., and Jonas, P. (2003). Kv3 potassium conductance is necessary and kinetically optimized for high-frequency action potential generation in hippocampal interneurons. J. Neurosci. *23*, 2058–2068.
24. Carter, B.C., and Bean, B.P. (2009). Sodium entry during action potentials of mammalian neurons: incomplete inactivation and reduced metabolic efficiency in fast-spiking neurons. Neuron *64*, 898–909.
25. Goldberg, E.M., Watanabe, S., Chang, S.Y., Joho, R.H., Huang, Z.J., Leonard, C.S., and Rudy, B. (2005). Specific functions of synaptically localized potassium channels in synaptic transmission at the neocortical GABAergic fast-spiking cell synapse. J. Neurosci. *25*, 5230–5235.
26. Rowan, M.J.M., and Christie, J.M. (2017). Rapid State-Dependent Alteration in Kv3 Channel Availability Drives Flexible Synaptic Signaling Dependent on Somatic Subthreshold Depolarization. Cell Rep. *18*, 2018–2029.
27. Armstrong, E.C., Caruso, A., Servadio, M., Andreae, L.C., Trezza, V., Scattoni, M.L., and Fernandes, C. (2020). Assessing the developmental trajectory of mouse models of neurodevelopmental disorders: Social and communication deficits in mice with Neurexin 1alpha deletion. Genes Brain Behav. *19*, e12630.
28. Jayabal, S., Ljungberg, L., Erwes, T., Cormier, A., Quilez, S., El Jaouhari, S., and Watt, A.J. (2015). Rapid Onset of Motor Deficits in a Mouse Model of Spinocerebellar Ataxia Type 6 Precedes Late Cerebellar Degeneration. eNeuro *2*. ENEURO.0094, 15.2015.
29. Shuvaev, A.N., Hosoi, N., Sato, Y., Yanagihara, D., and Hirai, H. (2017). Progressive impairment of cerebellar mGluR signalling and its therapeutic potential for cerebellar ataxia in spinocerebellar ataxia type 1 model mice. J. Physiol. *595*, 141–164.
30. Hong, J., Yoon, D., Nam, Y., Seo, D., Kim, J.H., Kim, M.S., Lee, T.Y., Kim, K.S., Ko, P.W., Lee, H.W., et al. (2020). Lipopolysaccharide administration for a mouse model of cerebellar ataxia with neuroinflammation. Sci. Rep. *10*, 13337.
31. Egorova, P.A., Gavrilova, A.V., and Bezprozvanny, I.B. (2020). Ataxic Symptoms in Huntington's Disease Transgenic Mouse Model Are Alleviated by Chlorzoxazone. Front. Neurosci. *14*, 279.

32. Sekirnjak, C., Martone, M.E., Weiser, M., Deerinck, T., Bueno, E., Rudy, B., and Ellisman, M. (1997). Subcellular localization of the K+ channel subunit Kv3.1b in selected rat CNS neurons. Brain Res. *766*, 173–187.

33. Shibata, R., Wakazono, Y., Nakahira, K., Trimmer, J.S., and Ikenaka, K. (1999). Expression of Kv3.1 and Kv4.2 genes in developing cerebellar granule cells. Dev. Neurosci. *21*, 87–93.

34. Liu, S.J., and Kaczmarek, L.K. (1998). The expression of two splice variants of the Kv3.1 potassium channel gene is regulated by different signaling pathways. J. Neurosci. *18*, 2881–2890.

35. Atzori, M., Lau, D., Tansey, E.P., Chow, A., Ozaita, A., Rudy, B., and McBain, C.J. (2000). H2 histamine receptor-phosphorylation of Kv3.2 modulates interneuron fast spiking. Nat. Neurosci. *3*, 791–798.

36. Stubbendorff, C., Hale, E., Day, H.L.L., Smith, J., Alvaro, G.S., Large, C.H., and Stevenson, C.W. (2023). Pharmacological modulation of Kv3 voltage-gated potassium channels regulates fear discrimination and expression in a response-dependent manner. Prog. Neuro-Psychopharmacol. Biol. Psychiatry *127*, 110829.

37. Leger, M., Grayson, B., Marsh, S., Alvaro, G., Large, C., Harte, M., and Neill, J. (2014). Kv3 channel modulation alleviates cognitive dysfunction and negative symptoms in an animal model of schizophrenia. Eur. Neuropsychopharmacol *2*, S516.

38. Chi, G., Liang, Q., Sridhar, A., Cowgill, J.B., Sader, K., Radjainia, M., Qian, P., Castro-Hartmann, P., Venkaya, S., Singh, N.K., et al. (2022). Cryo-EM structure of the human Kv3.1 channel reveals gating control by the cytoplasmic T1 domain. Nat. Commun. *13*, 4087.

39. Carpenter, J.C., Männikkö, R., Heffner, C., Heneine, J., Sampedro-Castañeda, M., Lignani, G., and Schorge, S. (2021). Progressive myoclonus epilepsy KCNC1 variant causes a developmental dendritopathy. Epilepsia *62*, 1256–1267.

40. Munch, A.S., Saljic, A., Boddum, K., Grunnet, M., Hougaard, C., and Jespersen, T. (2018). Pharmacological rescue of mutated K(v)3.1 ion-channel linked to progressive myoclonus epilepsies. Eur. J. Pharmacol. *833*, 255–262.

41. Porcello, D.M., Ho, C.S., Joho, R.H., and Huguenard, J.R. (2002). Resilient RTN fast spiking in Kv3.1 null mice suggests redundancy in the action potential repolarization mechanism. J. Neurophysiol. *87*, 1303–1310.

42. Ho, C.S., Grange, R.W., and Joho, R.H. (1997). Pleiotropic effects of a disrupted K+ channel gene: reduced body weight, impaired motor skill and muscle contraction, but no seizures. Proc. Natl. Acad. Sci. USA *94*, 1533–1538.

43. Espinosa, F., McMahon, A., Chan, E., Wang, S., Ho, C.S., Heintz, N., and Joho, R.H. (2001). Alcohol hypersensitivity, increased locomotion, and spontaneous myoclonus in mice lacking the potassium channels Kv3.1 and Kv3.3. J. Neurosci. *21*, 6657–6665.

44. Choudhury, N., Linley, D., Richardson, A., Anderson, M., Robinson, S.W., Marra, V., Ciampani, V., Walter, S.M., Kopp-Scheinpflug, C., Steinert, J.R., and Forsythe, I.D. (2020). Kv3.1 and Kv3.3 subunits differentially contribute to Kv3 channels and action potential repolarization in principle neurons of the auditory brainstem. J. Physiol. *598*, 2199–2222.

45. Kaar, S.J., Angelescu, I., Nour, M.M., Marques, T.R., Sharman, A., Sajjala, A., Hutchison, J., McGuire, P., Large, C., and Howes, O.D. (2022). The effects of AUT00206, a novel Kv3.1/3.2 potassium channel modulator, on task-based reward system activation: a test of mechanism in schizophrenia. Psychopharmacology (Berl) *239*, 3313–3323.

46. Angelescu, I., Kaar, S.J., Marques, T.R., Borgan, F., Veronesse, M., Sharman, A., Sajjala, A., Deakin, B., Hutchison, J., Large, C., and Howes, O.D. (2022). The effect of AUT00206, a Kv3 potassium channel modulator, on dopamine synthesis capacity and the reliability of [(18)F]-FDOPA imaging in schizophrenia. J. Psychopharmacol. *36*, 1061–1069.

47. Musselman, M., Huynh, E., Kelshikar, R., Lee, E., Malik, M., and Faden, J. (2023). Potassium channel modulators and schizophrenia: an overview of investigational drugs. Expert Opin. Investig. Drugs *32*, 471–477.

48. Kaar, S.J., Nottage, J.F., Angelescu, I., Marques, T.R., and Howes, O.D. (2023). Gamma Oscillations and Potassium Channel Modulation in Schizophrenia: Targeting GABAergic Dysfunction. Clin. EEG Neurosci. 155005942211486.

49. Stroobants, S., Gantois, I., Pooters, T., and D'Hooge, R. (2013). Increased gait variability in mice with small cerebellar cortex lesions and normal rotarod performance. Behav. Brain Res. *241*, 32–37.

50. Galliano, E., Gao, Z., Schonewille, M., Todorov, B., Simons, E., Pop, A.S., D'Angelo, E., van den Maagdenberg, A.M.J.M., Hoebeek, F.E., and De Zeeuw, C.I. (2013). Silencing the majority of cerebellar granule cells uncovers their essential role in motor learning and consolidation. Cell Rep. *3*, 1239–1251.

51. Chou, A.H., Yeh, T.H., Ouyang, P., Chen, Y.L., Chen, S.Y., and Wang, H.L. (2008). Polyglutamine-expanded ataxin-3 causes cerebellar dysfunction of SCA3 transgenic mice by inducing transcriptional dysregulation. Neurobiol. Dis. *31*, 89–101.

52. Guyenet, S.J., Furrer, S.A., Damian, V.M., Baughan, T.D., La Spada, A.R., and Garden, G.A. (2010). A simple composite phenotype scoring system for evaluating mouse models of cerebellar ataxia. J. Vis. Exp. *39*, 1787.

53. Kojic, M., Gaik, M., Kiska, B., Salerno-Kochan, A., Hunt, S., Tedoldi, A., Mureev, S., Jones, A., Whittle, B., Genovesi, L.A., et al. (2018). Elongator mutation in mice induces neurodegeneration and ataxia-like behavior. Nat. Commun. *9*, 3195.

54. Sugimoto, H., and Kawakami, K. (2019). Low-cost Protocol of Footprint Analysis and Hanging Box Test for Mice Applied the Chronic Restraint Stress. J. Vis. Exp. https://doi.org/10.3791/59027.

55. Ramachandran, P.S., Boudreau, R.L., Schaefer, K.A., La Spada, A.R., and Davidson, B.L. (2014). Nonallele specific silencing of ataxin-7 improves disease phenotypes in a mouse model of SCA7. Mol. Ther. *22*, 1635–1642.

56. Wilczynski, G.M., Konopacki, F.A., Wilczek, E., Lasiecka, Z., Gorlewicz, A., Michaluk, P., Wawrzyniak, M., Malinowska, M., Okulski, P., Kolodziej, L.R., et al. (2008). Important role of matrix metalloproteinase 9 in epileptogenesis. J. Cell Biol. *180*, 1021–1035.

57. Grecksch, G., Becker, A., Schroeder, H., Kraus, J., Loh, H., and Höllt, V. (2004). Accelerated kindling development in mu-opioid receptor deficient mice. Naunyn-Schmiedeberg's Arch. Pharmacol. *369*, 287–293.

58. Van Erum, J., Van Dam, D., and De Deyn, P.P. (2019). PTZ-induced seizures in mice require a revised Racine scale. Epilepsy Behav. *95*, 51–55.

59. Merrill, M.A., Clough, R.W., Jobe, P.C., and Browning, R.A. (2005). Brainstem seizure severity regulates forebrain seizure expression in the audiogenic kindling model. Epilepsia *46*, 1380–1388.

60. Martin, B., Dieuset, G., Pawluski, J.L., Costet, N., and Biraben, A. (2020). Audiogenic seizure as a model of sudden death in epilepsy: A comparative study between four inbred mouse strains from early life to adulthood. Epilepsia *61*, 342–349.

61. Wengert, E.R., Wenker, I.C., Wagner, E.L., Wagley, P.K., Gaykema, R.P., Shin, J.B., and Patel, M.K. (2021). Adrenergic Mechanisms of Audiogenic Seizure-Induced Death in a Mouse Model of SCN8A Encephalopathy. Front. Neurosci. *15*, 581048.

62. Tse, K., Beamer, E., Simpson, D., Beynon, R.J., Sills, G.J., and Thippeswamy, T. (2021). The Impacts of Surgery and Intracerebral Electrodes in C57BL/6J Mouse Kainate Model of Epileptogenesis: Seizure Threshold, Proteomics, and Cytokine Profiles. Front. Neurol. *12*, 625017.

63. Ting, J.T., Lee, B.R., Chong, P., Soler-Llavina, G., Cobbs, C., Koch, C., Zeng, H., and Lein, E. (2018). Preparation of Acute Brain Slices Using an Optimized N-Methyl-D-glucamine Protective Recovery Method. J. Vis. Exp. *132*, 53825.

## STAR★METHODS

### KEY RESOURCES TABLE

| REAGENT or RESOURCE | SOURCE | IDENTIFIER |
|---|---|---|
| Chemicals, peptides, and recombinant proteins | | |
| AUT00206 (AUT6) | Autifony Therapeutics Limited (Stevenage, UK). | N/A |
| Captisol | Captisol, Inc | N/A |
| Hydroxypropyl-methylcellulose | Sigma-Aldrich | 09963 |
| Tween-80 | Sigma-Aldrich | P1754 |
| DMSO | Sigma-Aldrich | 276855 |
| Pentylenetetrazol (PTZ) | Sigma-Aldrich | P6500 |
| Paraformaldehyde (PFA) | Electron Microscopy Sciences | 15713-S |
| Antibodies | | |
| Rabbit Calbindin D-28K antibody | Swant | CB38; RRID:AB_10000340 |
| Alexa Fluor 555 Goat anti-rabbit | Thermo Fisher | A21428; RRID:AB_2535849 |
| DAPI | Thermo Fisher | D3571; RRID:AB_2307445 |
| Experimental models: Organisms/strains | | |
| C57BL/6J | Jax | RRID:IMSR_JAX:000664 |
| B6.129P2-Pvalbtm1(cre)Arbr/J | Jax | RRID:IMSR_JAX:017320 |
| Rosa-CAG-LSL-tdTomato | Jax | RRID:IMSR_JAX:007914 |
| Software and algorithms | | |
| Pclamp 10 | Clampfit | N/A |
| GraphPad Prism 9 | GraphPad | RRID:SCR_002798 |
| MATLAB | Mathworks | 2021a |
| Biorender | Biorender.com | Agreement number: XZ249HQ8GU |
| HD-X02 | Data Sciences International, Inc. | N/A |
| Ponemah | Data Sciences International, Inc. | N/A |
| NeuroScore | Data Sciences International, Inc. | N/A |

### RESOURCE AVAILABILITY

#### Lead contact

Further information and requests for resources and reagents should be directed to and will be fulfilled by the lead contact, Ethan M. Goldberg (goldberge@chop.edu).

#### Materials availability

Materials generated in this study may be made available upon request. *Kcnc1*-p.Arg320His/+ mice generated in this study will be made available on request to the lead contact, Ethan M. Goldberg (goldberge@chop.edu), at The Children's Hospital of Philadelphia, but may require a payment and/or a completed Materials Transfer Agreement if there is potential for commercial application. For AUT00206, requests may be addressed to Charles H. Large (charles.large@autifony.com).

#### Data and code availability

All data are present in the manuscript or in the Supplementary Materials. This paper does not report original code. Any additional information required to reanalyze the data reported in this paper is available from the Lead Contact upon request.

### EXPERIMENTAL MODEL AND SUBJECT DETAILS

#### Experimental animals

All procedures and experiments were approved by the Institutional Animal Care and Use Committee at The Children's Hospital of Philadelphia and were conducted in accordance with the ethical guidelines of the National Institutes of Health. Male and female

mice were used in equal proportions. After weaning at P21, mice were group-housed with up to five mice per cage and maintained on a 12-h light/dark cycle with *ad libitum* access to food and water.

Mouse strains used in this study included: wild-type C57BL/6J (RRID: IMSR_JAX:000664), *Kcnc1*-p.Arg320His/+ (H/+ heterozygous) and *Kcnc1*-p.Arg320His/Arg320His (H/H; homozygous) mice on a C57BL/6J background; PV-Cre mice (B6.129P2-Pvalbtm1(cre)Arbr/J; RRID:IMSR_JAX:017320; on a C57BL/6J background); and tdTomato reporter/Ai14 mice (Rosa-CAG-LSL-tdTomato; RRID:IMSR_JAX:007914; on a C57BL/6J background). Female PV-Cre.tdT double homozygotes were crossed to male C57.*Kcnc1*-p.Arg320His/+ mice to generate *Kcnc1*.PV-Cre.tdT triple transgenic mice and WT.PV-Cre.tdT age-matched littermate controls on the same genetic background (back-crossed to C57BL/6J for at least 10 generations). The genotype of all mice was determined via PCR performed on tail snips obtained at P8 and was re-confirmed for each mouse after they were sacrificed for slice preparation or at experimental endpoint.

### Pharmacology

AUT00206 (AUT6, or 5,5-dimethyl-3-[2-(7-methylspiro[2H-benzofuran-3,1′-cyclopropane]-4-yl)oxypyrimidin-5-yl]imidazolidine-2,4-dione; Figure S1), was provided by Autifony Therapeutics Limited (Stevenage, UK). AUT6 was previously reported in other publications.[36,45–48] AUT6 used for *in vivo* studies was prepared in a suspension containing 20% by weight Captisol (a modified cyclodextrin; Captisol, Inc.), 0.5% weight by volume hydroxypropyl-methylcellulose K15M (Sigma-Aldrich), and 0.5% weight by volume Tween-80 (Sigma-Aldrich) in sterile water. For *in vitro* studies, AUT00206 was prepared as a 1 M stock solution in DMSO and further diluted to the required concentration. All final DMSO concentrations for *in vitro* studies was 0.01%. All control experiments *in vitro* and *in vivo* were performed with the identical concentration of vehicle.

## METHOD DETAILS

### Behavioral assays of motor function

All animals were habituated in the testing room for at least 30 min prior to performance of any behavior test. Unless specified, AUT00206 at 30 mg/kg or vehicle control was given via i.p. injection 45–60 min prior to all tests of motor function.

Motor coordination was tested on an accelerating Rotarod (MED Associates, Inc.; Vermont, USA) following an established protocol.[49] Baseline performance was tested one week prior to the treatment trial. After two training sessions at a constant speed (6 rpm; 2 min), four 5-min trials were performed with a 2-min inter-trial interval. During these trial sessions, mice were placed on a rotating rod that accelerated from 6 to 60 rpm in 5 min, and time to fall was recorded.

For the Elevated Beam Walk Test, mice were placed at one end of a 1.5 m long X 1.0 or 0.75 cm diameter beam placed between two platforms located 30 cm above the floor. Mice were recorded by video as they traversed the beam, and footfalls were counted post-hoc, blind to genotype. Trials were repeated 3 times per mouse, with a 5-min interval between trials.[50]

The Tail Suspension Test measured the presence or absence of the normal extension reflex of the hind limbs typically observed when a mouse is suspended by its tail. Hindlimb clasping is a sensitive marker of cerebellar dysfunction or degeneration in mouse models, including cerebellar ataxia.[51,52] The mouse was gently removed from the home cage and suspended by the tail for 25 s. The entire session was video recorded. The total duration of hindlimb clasping was documented.

The Ledge Test is another measure of coordination that is a measure of impaired coordination in mice with cerebellar ataxia.[52,53] Briefly, mice are lifted from the cage floor and placed on the edge of the home cage. Each mouse then walks from one end of the cage to the other along the ledge for three trials, with performance recorded via video. All tests were scored on a scale of 0–3: a score of 0, the mouse walks along the ledge without loss of balance; 1, the mouse loses its footing while walking along the ledge but does not fall; 2, a mouse does not effectively use its hind legs, and/or is unable to land on its paw(s) when descending the ledge into the cage; 3, the mouse falls off the ledge while traversing the ledge.[52]

Paw-Print Analysis is a method to assess gait and identifies gait impairment in mice with motor dysfunction.[54,55] Briefly, to obtain at least five sets of paw prints from both front and hind paws, a runway was set up using a piece of white paper (13.97 cm × 96.52 cm), with a dark goal box at the distal end of the paper, and walls on both side of the runway. Prior to applying ink to mouse's paws, each mouse was allowed three training sessions to reach the goal box. In the test session, the forepaws of the mouse were labeled with green ink while the hind paws were labeled with red ink. Then mouse is immediately put on the proximal end of the paper to walk to the goal box. Gait parameters were obtained as per established protocols.[54]

### Pentylenetetrazol (PTZ) seizure threshold test

A PTZ kindling protocol was performed as described to assess kindling epileptogenesis.[56] Briefly, PTZ was administered once every other day for 24 days at 30 mg/kg starting at P30. Mice were monitored for 30 min for behavioral signs of seizure as described by the modified Racine scale.[56–58] This subthreshold PTZ dose was titrated to never elicit seizure on the first injection in wild-type mice regardless of sex or strain and to lead to kindling epileptogenesis in approximately 50% of mice after 12 doses. Sensitization was defined as death or two sequential sessions with a tonic-clonic (stage 5) seizure.[58] The number of injections to reach a sensitized state for each mouse was reported in survival curves. AUT00206 at 30 mg/kg or vehicle was given through oral gavage at 45–60 min before PTZ injection (i.p.) on the same day.

### Audiogenic seizures

To test for the presence of high-intensity sound-induced audiogenic seizures, mice age P18-20 were placed in a custom-made cylindrical Plexiglass chamber (40 cm in diameter and 50 cm in height) with a siren mounted inside the lid. Sound was delivered at 130 dB for 1 min[59] and mice exhibited an all-or-nothing generalized tonic-clonic (stage 5) seizure.

To test for high frequency sound-induced audiogenic seizures, mice at P18-20 were placed in a holding chamber and subjected to ultrasonic noise (Branson 200) as described previously,[60,61] until the animal exhibited a seizure, or 50 s expired.

### EEG recordings

Continuous video EEG recording was performed with a wireless EEG recording system (Data Sciences International, St. Paul, MN). The surgical procedure was similar to published protocols.[62] Briefly, mice were anesthetized with isoflurane, and four burr holes (two in each hemisphere) were made through the skull corresponding to the motor and barrel cortex. A telemetry device containing four electrode leads (DSI HD-X02) was placed subcutaneously on the back. 4 mm of insulation was removed from the ends of the positive and negative leads. Then, a V-shape bend was made manually in the coiled wires to create a flat terminal end, which was inserted through the burr holes to create contact with the dura. Electrodes were secured to the skull using quick adhesive cement (C&B-Metabond, Parkell Inc, Brentwood, NY). The incision was then sutured (Pivetal WEBCRYL Sutures, Patterson Veterinary, Houston, TX), and OTC Generics Triple Antibiotic Topical Ointment (Patterson Veterinary, Houston, TX) was applied to the scalp surface to facilitate wound healing. Animals were then returned to single-housed cages and were given hydrogel to facilitate recovery overnight. Synchronized video and EEG monitoring of the mice was conducted using the Ponemah Software System (DSI, St Paul, MN) according to the experimental design. Acquisition frequency for EEG was 500 Hz. For the AUT00206 treatment trial, three days of baseline monitoring was conducted. Then, EEG signals were analyzed immediately using NeuroScore (DSI) to determine whether spontaneous seizure was observed. Only mice with two or more detected seizures in 72 h were included in the AUT6 treatment study.

### Cell culture and transfection

Cell culture, transfections, and ion channel electrophysiology experiments were performed using HEK-293T cells. Cells were grown at 37°C with 5% CO2 in Dulbecco modified Eagle medium supplemented with 10% fetal bovine serum, 2 mM L−glutamine, and penicillin (50 U/mL)–streptomycin (50 μg/mL). HEK-293T cells were co-transfected with 0.1 μg of p.GFP-IRES reporter construct and 0.2 μg total of pcDNA3.1-*KCNC1* (reference sequence NM_001112741.2) and WT vs. p.Arg320His vs. WT + *KCNC1*-p.Arg320His in a 1:1 ratio using 10 μL of PolyFect transfection reagent (QIAGEN) in 35-mm culture dishes following the manufacturer's instructions. Cells were then incubated for 24h after transfection prior to electrophysiological recording. Transfected cells were then trypsinized and seeded on 35 mm dishes to a density allowing single GFP-positive cells to be identified and targeted for recording. After 4 h at 37°C in 5% CO2, cells were washed once with extracellular Tyrode solution for 5 min prior recording.

### Voltage-clamp recording of ionic currents

Voltage-clamp recordings of HEK-293T cells were carried out in the whole cell configuration at room temperature (~22°C). Whole-cell patch clamp was performed at room temperature using an Axopatch 200B amplifier (Molecular Devices, Sunnyvale, CA) in an extracellular Tyrode's solution consisting of the following: 150 mM NaCl, 2 mM KCl, 1.5 mM $CaCl_2$, 2 mM $MgCl_2$, 10 mM HEPES and 10 mM glucose; pH was adjusted to 7.4 with NaOH. Intracellular solution contained, in mM: 125 KCl, 25 KOH; 1 $CaCl_2$, 2 $MgCl_2$, 4 $Na_2$-ATP, 10 EGTA, 10 HEPES, with pH adjusted to 7.2 with KOH and osmolarity to 305 mOsm/L with sucrose. Patch pipettes were fashioned from thin-walled borosilicate glass (Harvard apparatus, Holliston, MA) and fire-polished (Zeitz) to a resistance of 1.7–2.5 MΩ in the whole cell configuration. Currents were filtered at 5 kHz (−3 dB, eight-pole low-pass Bessel filter) and digitized at 30 kHz (Digidata 1550B). Data were acquired using Clampex and analyzed with Clampfit 11.1 (Axon Instruments, San Jose, CA). Potassium currents were measured by performing 100 m step depolarizations to between −40 and +40 mV in increments of 5 mV from a holding potential of −80 mV, and the current–voltage relation was constructed; this was followed by a 100 m pulse to −40 mV to facilitate measurement of tail current. Conductance was normalized, plotted against voltage, and fit with a Boltzmann function to determine $V_{1/2}$ of activation.

Heterologous expression in Xenopus oocytes and two-electrode voltage clamping (TEVC) experiments were conducted and analyzed as reported previously.[38] Oocytes were harvested in accordance with a protocol approved by the IACUC at Thomas Jefferson University. AUT00206 was dissolved in extracellular recording solution at the desired final concentration and applied to the oocyte in the recording chamber by means of a gravity-driven perfusion system. All TEVC recordings were conducted at room temperature (22°C–24°C).

### Acute brain slice preparation

Mice were deeply anesthetized with 5% isoflurane in oxygen and transcardially perfused with ice-cold protective recovery solution[63] containing, (in mM): KCl, 2.5; $NaHPO_4$, 1.25; HEPES: 20; N-Methyl-D-glutamine (NMDG), 93; L-ascorbic acid (sodium salt), 5; thiourea, 2; sodium pyruvate, 3; $CaCl_2$, 0.5; $MgSO_4$, 10; D-glucose, 25; N-acetyl-L-cysteine, 12; $NaHCO_3$, 30; with pH adjusted to 7.30 with HCl and osmolarity adjusted to 310 mOsm, and equilibrated with 95% $O_2$ and 5% $CO_2$. The brain was rapidly removed to cold recovery solution, then blotted dry and glued to the platform of a Leica VT-1200S vibratome with cyanoacrylate glue and sectioned at 300 microns. Slices recovered in the same solution for 30 min at 32°C and were then maintained at room temperature for up to 3 h

prior to recording. Slices were transferred to the stage (Scientifica) of an upright microscope (Leica DM-6) and perfused at 3 mL/min with standard (recording) artificial cerebrospinal fluid (aCSF) containing (in mM): NaCl, 125; KCl, 2.5; $MgSO_4$, 2; NaH2$PO_4$, 1.25; $CaCl_2$, 2; D-glucose, 20; $NaHCO_3$, 26, using a pump (Gilson Minipuls 3). Solution was bubbled continuously with carbogen to maintain a pH of 7.30 and warmed to 30 ± 1°C using an in-line heater.

### Electrophysiological recordings in acute brain slice

Cerebellar granule cells and Purkinje cells were identified by location and morphology under infrared differential interference contrast (IR-DIC). PV-INs from layer 2–4 primary somatosensory cortex were identified by tdTomato expression in PV-Cre.tdT mice and visualized with epifluorescence. Patch pipettes were pulled from borosilicate glass (Sutter) using a two-stage pipette puller (Narishige) and filled with intracellular solution containing (in mM): K-gluconate, 130; KCl, 6.3; $MgCl_2$, 2; HEPES, 10; EGTA, 0.5; Phosphocreatine-Tris2, 10; ATP-Mg; 4; GTP-Na, 0.3; pH was adjusted to 7.30 with KOH, and osmolarity adjusted to 290 mOsm. Pipettes with a resistance of 3–4 MΩ when filled were used to record cerebral cortex PV-INs, pyramidal cells, and cerebellar Purkinje cells; pipettes with a resistance of 6–8 MΩ when filled were used to record cerebellar granule cells.

For analysis of unitary synaptic transmission, post-synaptic cells were recorded with an internal solution containing (in mM): K-gluconate, 65; KCl, 65; $MgCl_2$, 2; HEPES, 10; EGTA, 0.5; Phosphocreatine-Tris2, 10; ATP-Mg; 4; GTP-Na, 0.3; pH 7.30 and osmolarity 290 mOsm. Unitary IPSCs were obtained via 2–6 simultaneous patch clamp recordings from neurons located within 100 μm of one another in slices from young mice (P16-21) and recorded as inward currents from a holding potential of −80 mV. Voltage was sampled at 100 kHz with pClamp software and a MultiClamp 700B amplifier (Molecular Devices), low-pass filtered at 10 kHz, and digitized using a DigiData 1550B. Recordings were discarded if the cell had an unstable resting membrane potential and/or a membrane potential greater (less negative) than −55 mV, or if access resistance increased by > 20% during the recording. We did not correct for liquid junction potential.

To record evoked EPSCs in Purkinje cells, parallel fibers were stimulated with a bipolar stimulating electrode fashioned from a theta glass pipette positioned at the surface of the slice in the central third of the cerebellar molecular layer. Trains of pulses were generated by a Master-9 Programmable Pulse Stimulator (A.M.P.I.; Jerusalem, Israel). A train of 200 μs pulses was generated at 20 Hz for 1 s (i.e., 20 pulses). Identical stimulus parameters and pipettes were used between experiments to achieve comparable numbers and density of active parallel fibers, and recordings were performed blind to genotype.

### Immunohistochemistry

Mice were deeply anesthetized with isoflurane, then transcardially perfused with 10–15 mL of 4% paraformaldehyde (PFA) in PBS and postfixed for 24 h. 50 μm coronal sections through sensorimotor neocortex were cut using a vibratome (Leica VT1200S). After washing in PBS, the slices were incubated in blocking solution (5% normal goat serum, 0.3% Triton X-100 in PBS) for 1 h at room temperature to decrease nonspecific staining, and then washed in PBS. The sections were then transferred into primary antibody solution containing rabbit Calbindin D-28K antibody (1:1000; Swant CB38) in blocking solution at 4°C overnight. Next, sections were washed 3 times with 0.1% Triton X-100 in PBS and incubated with secondary antibody Alexa Fluor 555 (1:1000; Thermo Fisher A21428) and 4 ng/mL DAPI (Thermo Fisher, D3571) in blocking solution for 2h at room temperature and then washed 3 times with 0.1% Triton X-100 in PBS and 1 time in milliQ $H_2O$. Sections were finally mounted on glass slides and coverslipped using ProLong Gold Antifade Mountant (Life Technologies P36939). 5 μm thick z stack images were acquired at 1 μm intervals using a confocal microscope (Leica SP8) equipped with 20X and 40X objectives. Image processing was performed with LAF (Leica) and ImageJ software (NIH, USA).

### Data analysis

All electrophysiological analysis, if not specified, was performed manually in Clampfit or using custom routines written in MATLAB. Resting membrane potential ($V_m$) was calculated using the average value of a 600 ms or 1 s sweep with no direct current injection. Input resistance ($R_m$) was calculated using the slope of the response to hyperpolarizing current injections near rest using $R_m = V/I$. AP threshold was calculated as the value at which the derivative of the voltage (d$V$/dt) first reached 10 mV/ms. Spike height refers to the absolute maximum voltage value of an individual AP, while spike amplitude was calculated as the difference between spike height and AP threshold for a given AP. AP rise time is the time from AP threshold to the peak of the AP. AP half-width (AP ½-width) is defined as the width of the AP (in ms) at half-maximal amplitude. AP afterhyperpolarization (AHP) amplitude is calculated as the depth of the afterhyperpolarization (in mV) relative to AP threshold. AHP time is calculated as the time from AP threshold to the maximum (most negative) depth of the fast, deep AHP, characteristic of PV-INs. Unless indicated, all quantification of single spike properties was done using the first AP elicited at rheobase, or, for PV-INs with a delay to first spike (Goldberg et al., 2008), for the first spike during repetitive firing. Rheobase was determined as the minimum current injection that elicited action potentials using a 600 ms sweep at 2 pA intervals for cerebellar granule cells and 50 pA intervals for neocortical PV-INs and pyramidal cells. Maximal instantaneous firing was calculated using the smallest interspike interval (ISI) elicited during trains of action potentials in response to near-maximal current injection. Maximal steady-state firing was defined as the maximal mean firing frequency during the last 300 ms of a suprathreshold 600 ms current injection, with a minimum requirement for a spike being an amplitude of 40 mV with a clear AP threshold of d$V$/dt greater than 10 mV/ms and height overshooting at least 0 mV.

The amplitude of the unitary E or IPSC was calculated as the difference between baseline and peak from the average of 20 consecutive sweeps obtained with a 15 s inter-sweep interval to facilitate recovery from short-term synaptic depression or facilitation. The paired pulse ratio (PPR) was calculated from this data as the ratio of the second ($PSC_2$) to the first PSC. At 40 and 120 Hz, the amplitude of the subsequent PSCs in the train was calculated as the difference between the peak amplitude and the extrapolation of the single exponential fit to the decay of the preceding PSC. Unitary PSC failure was defined as the absence of a transient current greater than 5 pA occurring within 5 ms after the presynaptic AP.

EEG data is analyzed using spike train detector module in NeuroScore software. The spikes are detected by scanning EEG signal for amplitude changes crossing a set threshold. A continuous series of detected spikes over a defined time period were defined as a spike train. The minimum spike train duration is set to 5 s. All the detected spike trains along with the recorded videos are manually confirmed as seizures via review of video and EEG.

## QUANTIFICATION AND STATISTICAL ANALYSIS

Unless indicated, all comparisons between +/+, H/+, and H/H were performed using one-way ANOVA with post-hoc Šídák's Test to correct for multiple comparisons. Comparisons between +/+ and H/+ were performed using an unpaired Student's *t* test if the data passed a D'Agostino & Pearson Test; otherwise, a Mann-Whitney Test was used. For pharmacological data (before/after AUT00206), a paired t-test was used. Survival curves from the PTZ kindling study or mouse survival based on genotypes were analyzed with a Mantel-Cox Test. Statistical tests and plots were performed using GraphPad Prism 9 (RRID:SCR_002798). Statistical significance was defined as $p < 0.05$ after *post-hoc* correction with the p value reported exactly. All average values are Mean ± SEM. Numbers for mice (*N*) and cells and synaptic connections (*n*) are reported in the Figure legends and in Table S1.

**Cell Reports Medicine, Volume *5***

## Supplemental information

# Targeted therapy improves cellular dysfunction, ataxia, and seizure susceptibility in a model of a progressive myoclonus epilepsy

**Huijie Feng, Jerome Clatot, Keisuke Kaneko, Marco Flores-Mendez, Eric R. Wengert, Carly Koutcher, Emily Hoddeson, Emily Lopez, Demetrius Lee, Leroy Arias, Qiansheng Liang, Xiaohong Zhang, Ala Somarowthu, Manuel Covarrubias, Martin J. Gunthorpe, Charles H. Large, Naiara Akizu, and Ethan M. Goldberg**

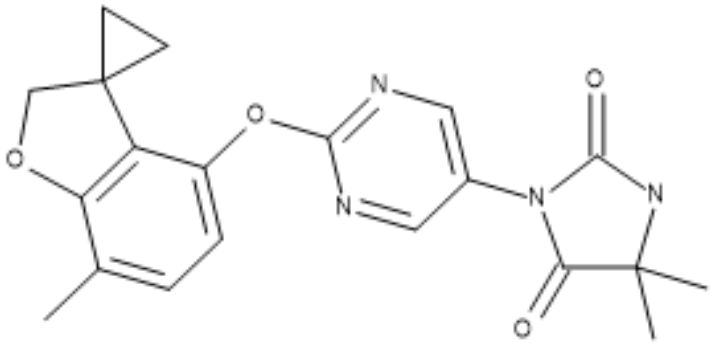


**Figure S1. Chemical structure of AUT00206 (AUT6, or 5,5-dimethyl-3-[2-(7-methylspiro[2H-benzofuran-3,1'-cyclopropane]-4-yl)oxypyrimidin-5-yl]imidazolidine-2,4-dione).** Related to STAR★ Methods.

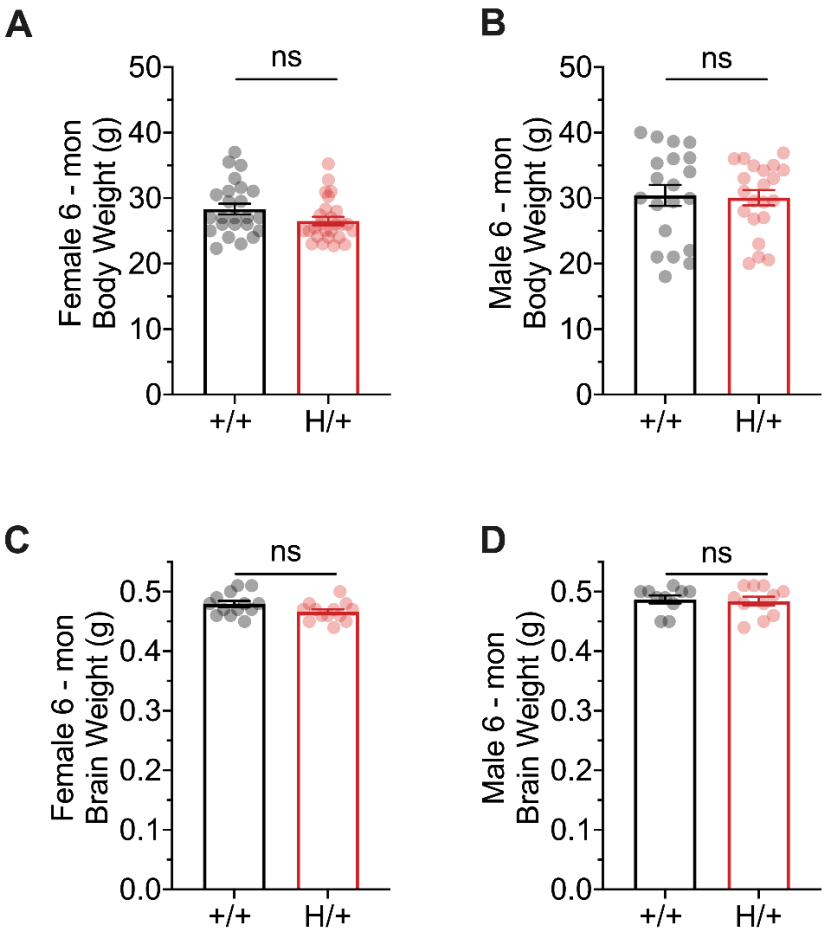


**Figure S2. Body and brain weight show no genotype difference in either sex.** Related to Figure 1.

(A-B) At 6 months of age, there is no difference in body weight between WT and H/+ mice for either females (A) or males (B).

(C-D) There is no difference in brain weight between WT and H/+ mice for either females (C) or males (D).

Data are presented as mean ± SEM. Statistical analyses: unpaired Student's t-test.

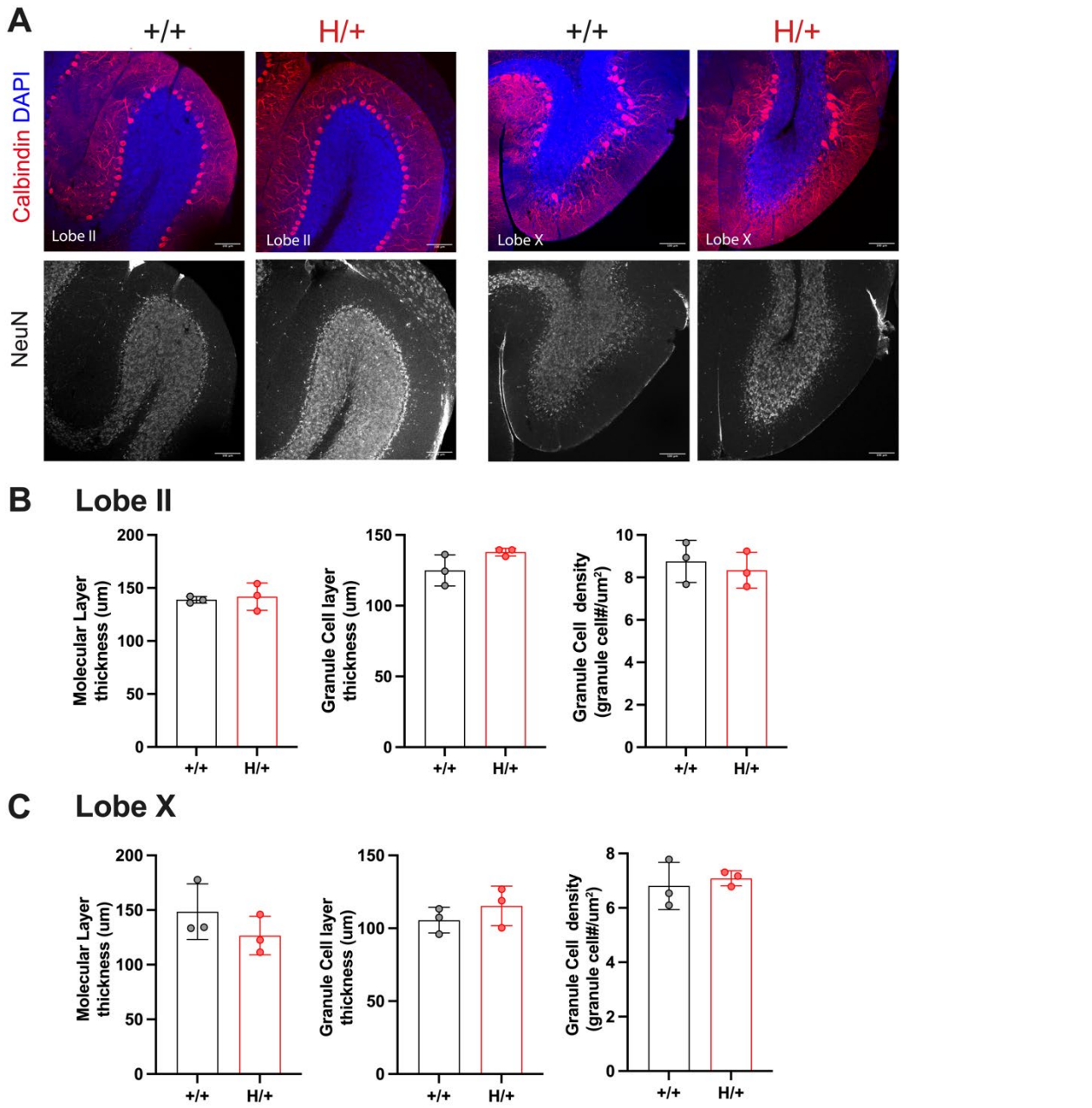


**Figure S3. 9-month-old H/+ mice show no loss of cerebellar granule cells or Purkinje cells.** Related to Figure 1.

(A) Examples of representative cerebellar lobes (Lobe II and Lobe X) for +/+ and H/+ mice at 9 months of age.

Quantification of cerebellar layer thickness of 9-month-old H/+ mice and WT littermate controls shows no significant difference in molecular layer sickness, granule cell layer thickness and granule cell density in Lobe II (B) and Lobe X (C).

Data are presented as mean ± SEM. Statistical analyses: unpaired Student's t-test.

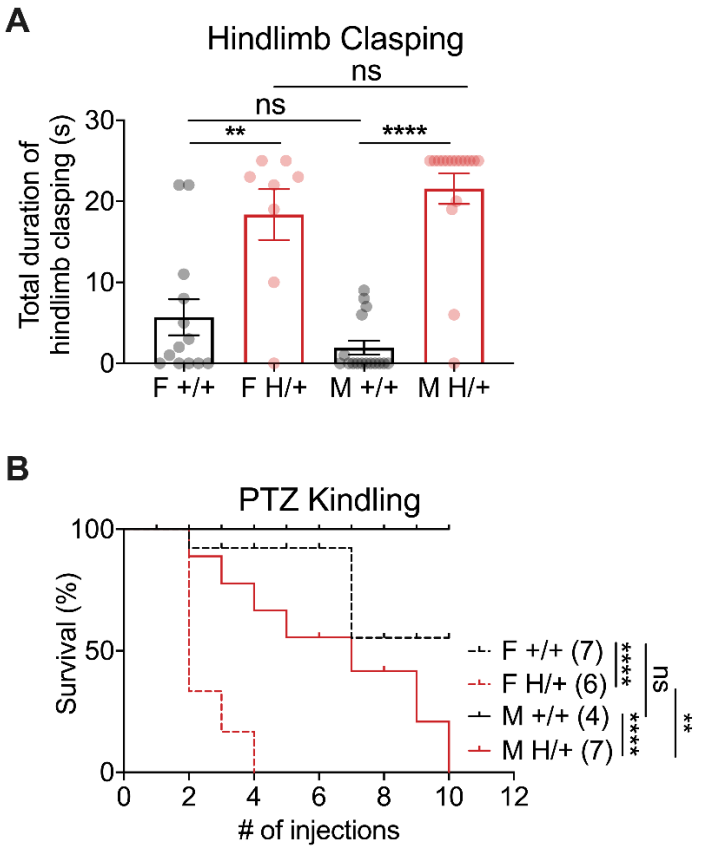


**Figure S4. The main disease-related phenotypes identified in H/+ mice are present in both males and females.** Related to Figure 3.

(A) Hindlimb clasping is an indicator of cerebellar dysfunction; genotype differences between H/+ and WT mice persist in a subgroup analysis of males and females only. There is no genotype difference in the performance of either male or female mice.

(B) Accelerated PTZ kindling epileptogenesis – a measure of cerebral cortex hyperexcitability and propensity to seizure – is present in both male and female H/+ mice relative to WT. Female H/+ mice are more prone to PTZ-induced kindling epileptogenesis than male H/+ mice.

Data are presented as mean ± SEM. Statistical analyses: (A) one-way ANOVA with Šídák's multiple comparison test; (B) Mantel-Cox Test;**, $p < 0.01$; ****, $p < 0.0001$.

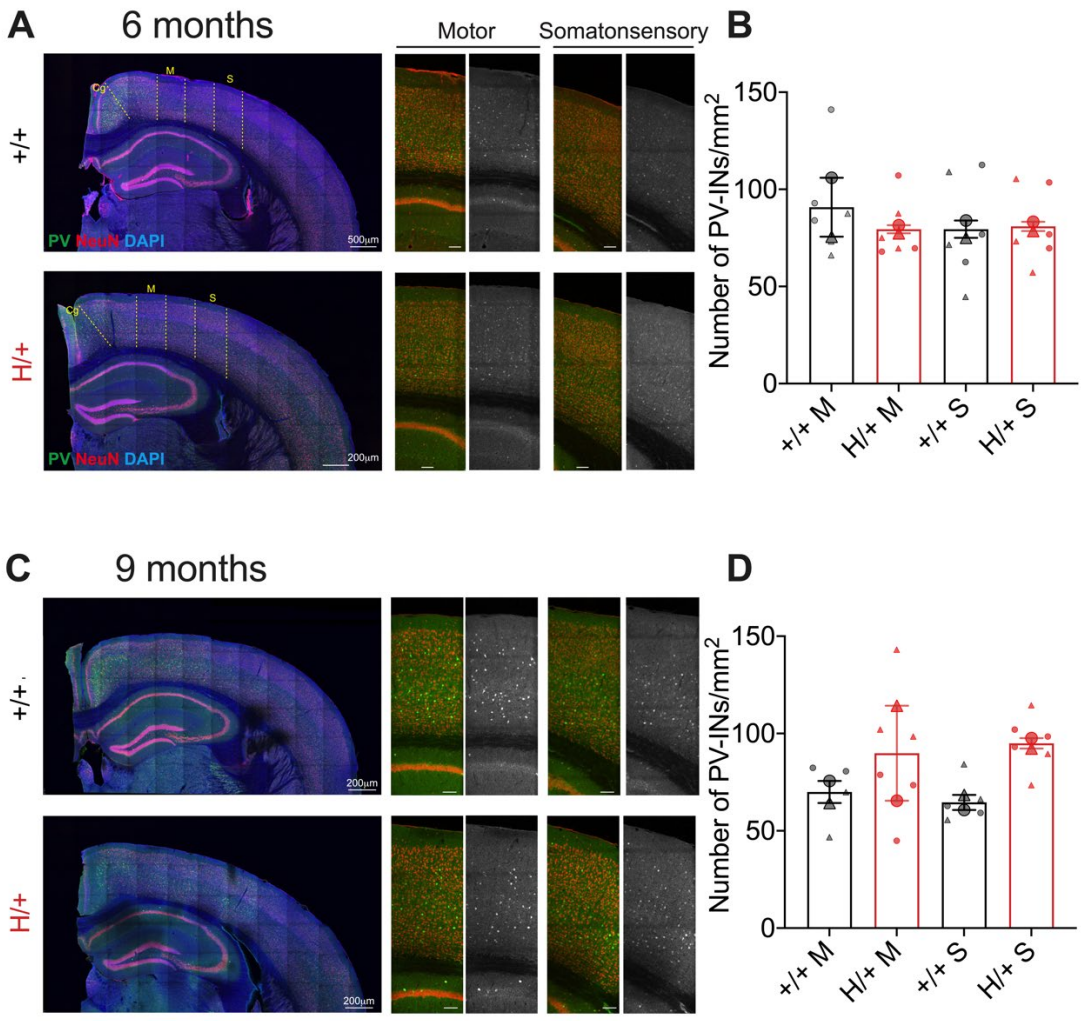


**Figure S5. Normal neocortical GABAergic PV-IN numbers in H/+ mice**. Related to Figure 1.

(A, C) The number of PV-INs is normal in H/+ mice. Shown is a representative image of motor and somatosensory neocortex demonstrating immunostaining with anti-pavalbumin and anti-NeuN antibodies and counterstaining with DAPI in coronal sections of 6- (A) or 9-month-old (C) +/+ and H/+ mice.

(B, D) Bar graphs show summary data, presented as mean (*large dots*) ± SEM of PV-IN density in $n = 2$ mice of each genotype (calculated from the average of 3 sections per mouse; *small dots*).

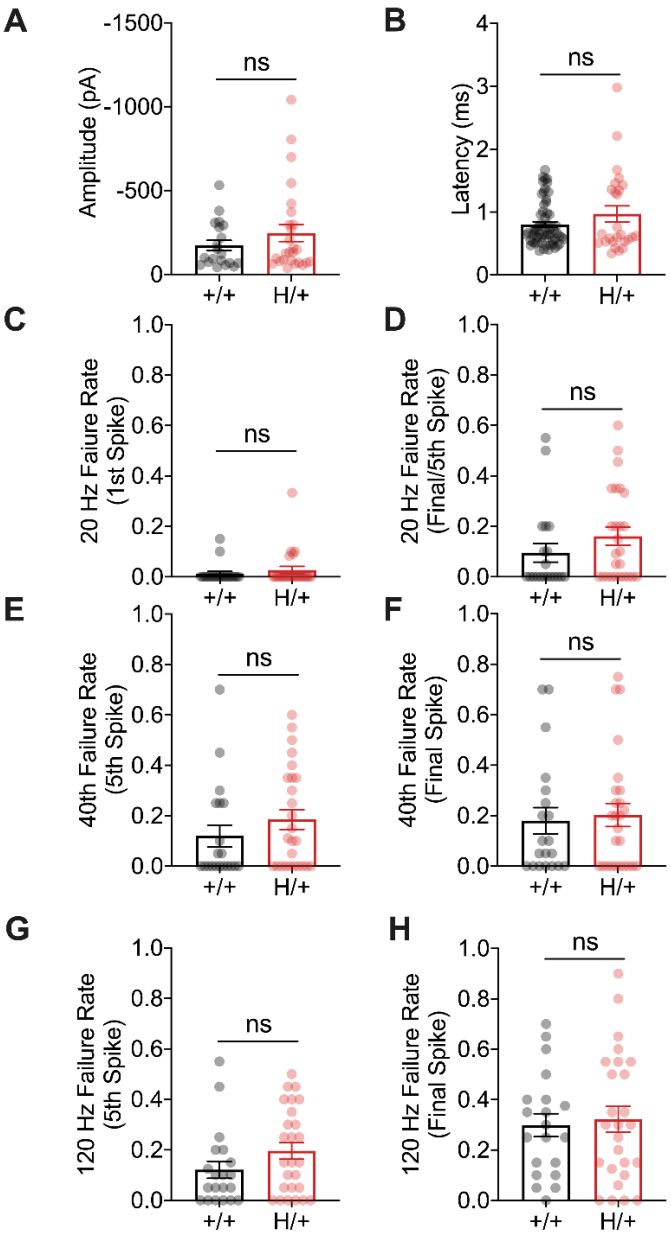


**Figure S6. Features of unitary synaptic transmission at PV-IN:principal cell synapses in H/+ versus WT mice at P16-21.** Related to Figure 5.

There is no significant difference in average unitary inhibitory postsynaptic current (uIPSC) amplitude (A) or latency (B) between +/+ and H/+ mice at P16-21. (C-H) Failure rate with 20, 40 or 120 Hz stimulation also shows no significant difference between +/+ and H/+ mice. Data are presented as mean ± SEM. Statistical analyses: unpaired Student's t-test.

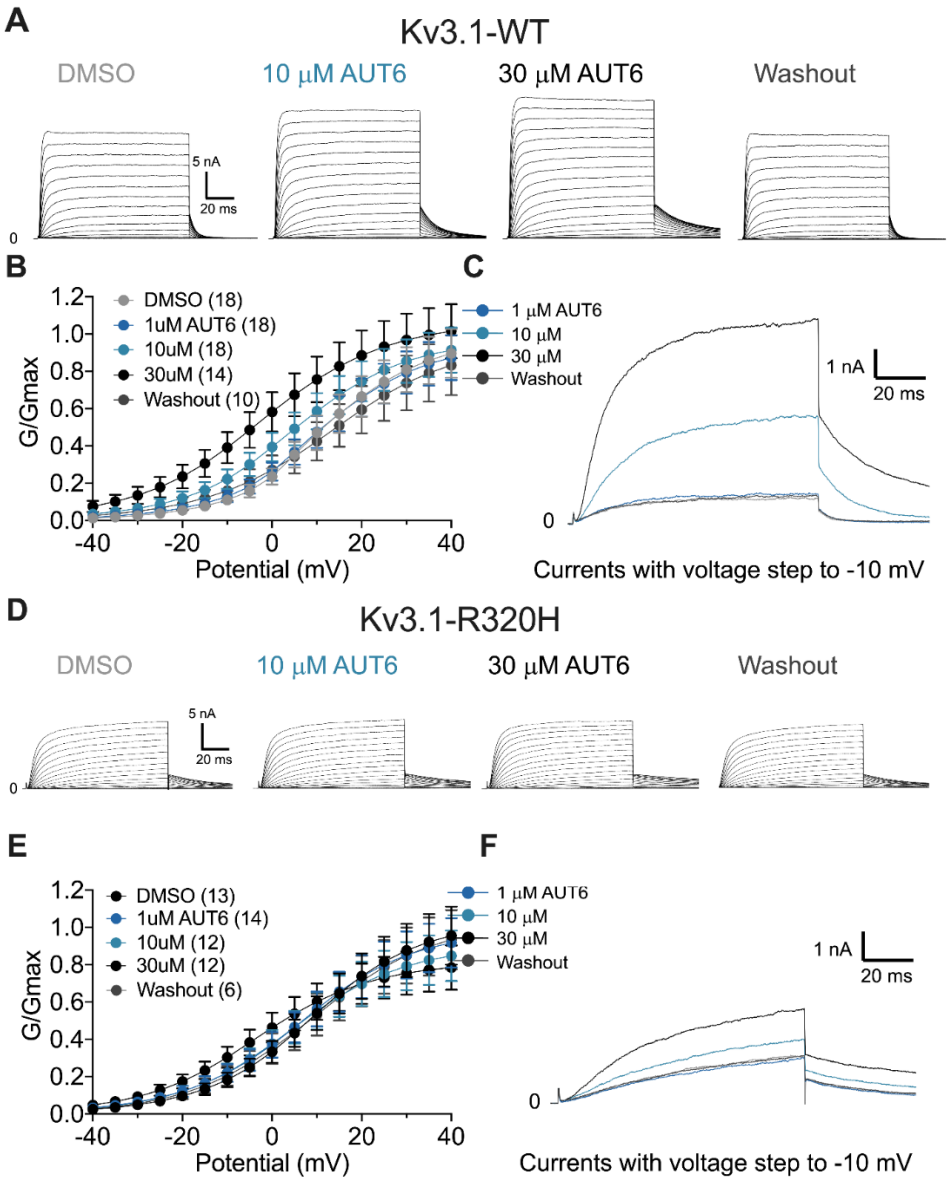


**Figure S7. Biophysical properties of Kv3.1-WT and Kv3.1-Arg320His with activation by AUT00206.** Related to Figure 6.

(A-C) Data for Kv3.1-WT. Shown are representative currents of HET-293T transiently transfected with Kv3.1-WT alone in response to increasing concentrations of AUT00206 along with washout (A), and corresponding with G/Gmax curves (B). (C) Overlay of currents in response to a voltage step to -10 mV to highlight the effect of AUT00206.

(D-F) as in (A-C), but for HET-293T cells transiently transfected with the Kv3.1-Arg320His variant alone. Note lower peak and steady-state currents relative to Kv3.1-WT but with clear activation by AUT00206 in the raw traces (D) and G/Gmax curves (E). The effect of AUT00206 on Kv3.1-Arg320His is highlighted via overlay of the response to voltage steps to -10 mV (F).

Data are presented as Mean ± SEM.

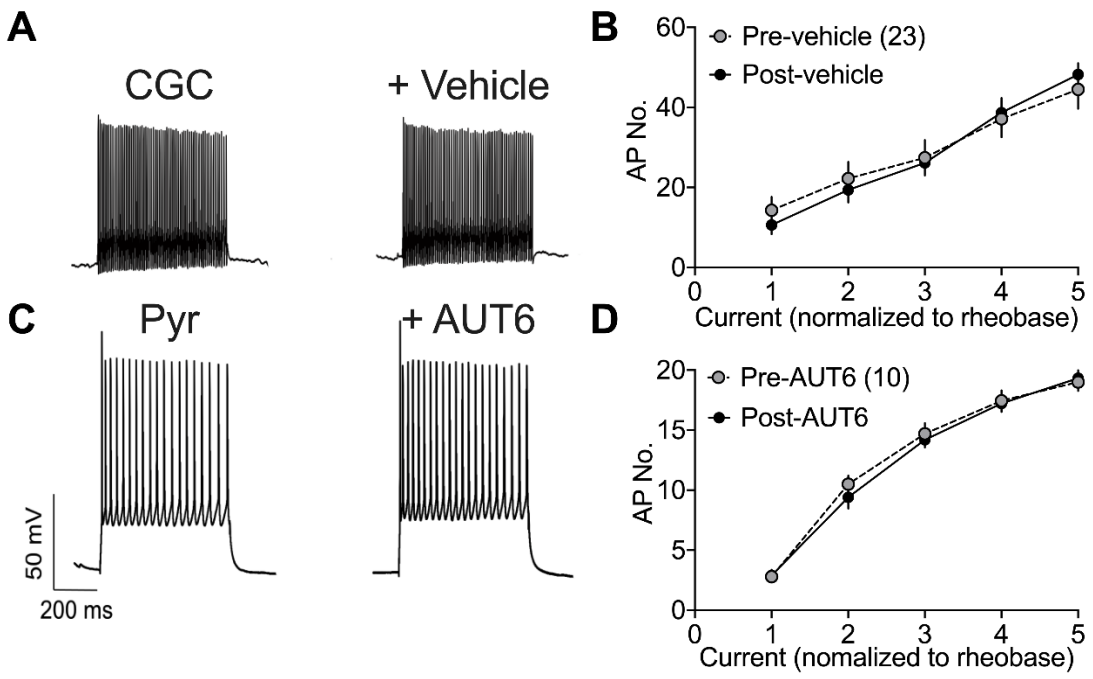


**Figure S8. Specificity of AUT00206 for Kv3-expressing neurons**. Related to Figure 6.

(A-B) Vehicle has no effect on the electrical excitability of cerebellar granule cells.

(C-D) AUT00206 has no effect on neocortical pyramidal neurons, which do not express Kv3 channels.

Data are presented as Mean ± SEM. Statistical analyses: Two-way ANOVA with Šídák's multiple comparison test.

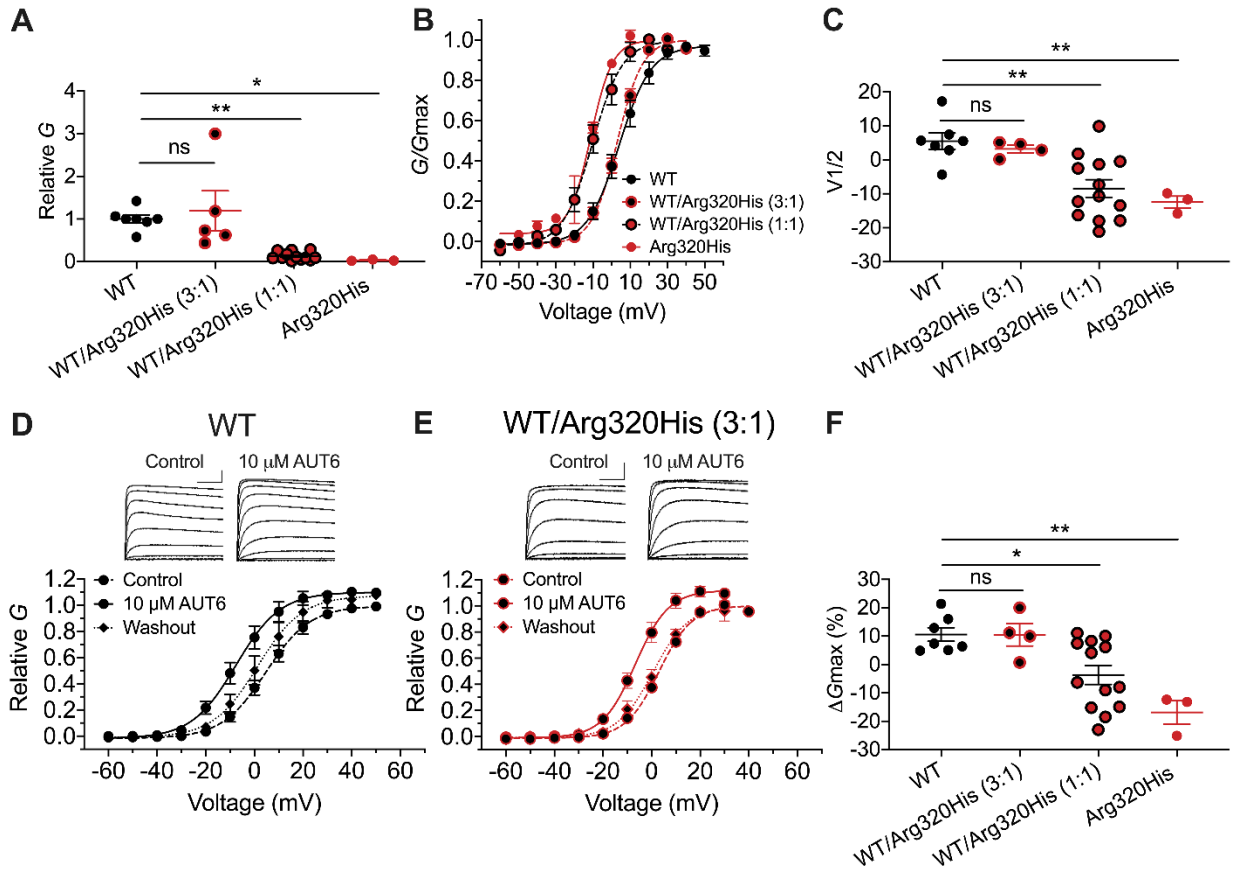


**Figure S9. Properties of human *KCNC1*-p. Arg320His and effect of AUT00206 in *Xenopus* oocytes.** Related to Figure 6.

Shown are results of two-electrode voltage-clamp recordings of wild-type and variant *KCNC1* expressed in *Xenopus* oocytes.

(A) Plot of relative conductance (*G/Gmax*; y-axis) for wild-type Kv3.1 (WT; *black circles*), Kv3.1- Arg320His (Arg320His; *red circles*), and 3:1 (*black circles with red borders*) or 1:1 mixtures of WT and Arg320His RNA (*red circles with black borders*). Note that Arg320His alone produces essentially no current, while mixtures of WT and Arg320His produce intermediate levels of current consistent with a dominant negative effect of the Arg320His -containing subunit. Note that identical amounts of RNA were injected in all experimental conditions at a concentration of 36 ng/uL.

(B) *G-V* plots showing a left shift in the voltage dependence of activation for Arg320His alone and with a 1:1 mixture with WT (but not at 3:1 mixture), and increased conductance at/around 0 mV for Arg320His and 1:1.

(C) Quantification of (B) with plot of voltage at half-maximal activation ($V_{1/2}$) for each group.

(D-F) AUT00206 produces increased conductance of WT Kv3.1 (D) and WT/Arg320His at a 3:1 ratio (E), but not with a 1:1 ratio. R320H alone produces very small currents (*not shown*). (F) quantification of relative changes in *G*max from the data in D and E. (D-E*)*.
Data are presented as Mean ± SEM. Statistical analyses: One-way ANOVA with Šídák's multiple comparison test, * $p< 0.05$; ** $p < 0.01$.

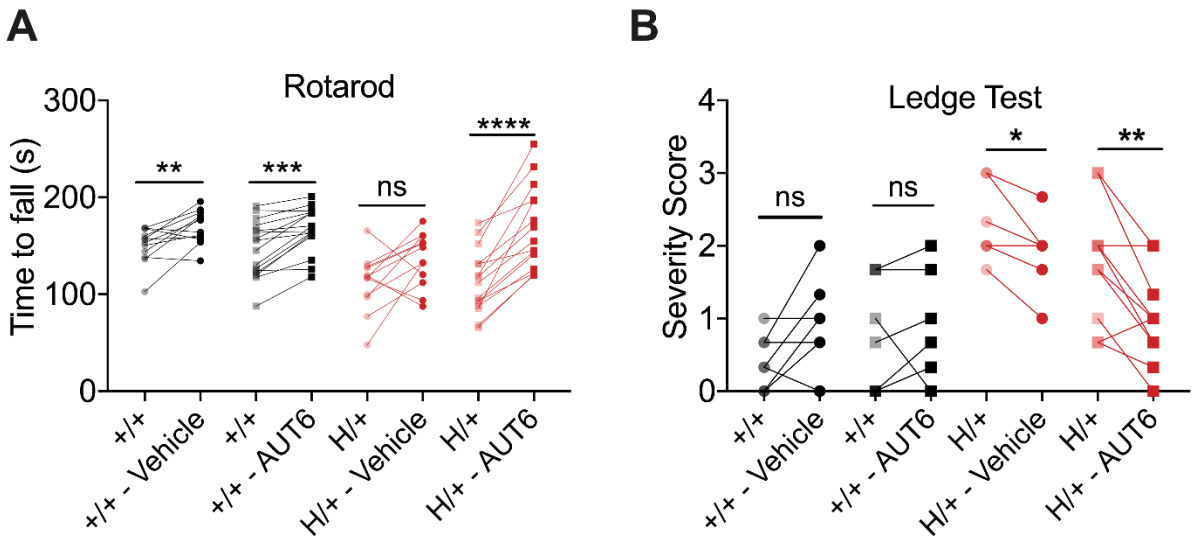


**Figure S10. Effect of a single i.p. dose of AUT00206 (30 mg/kg) on the performance of WT and H/+ mice on the Rotarod and Ledge Test.** Related to Figure 6.

While we did observe a learning effect in the motor behavioral tests, a single i.p. injection of 30 mg/kg AUT6 still significantly improved the performance of 6-month-old mice on the Rotarod (A) and in the Ledge Test (B).

Data are presented as mean ± SEM. Statistical analysis via paired t-test. * $p < 0.05$, ** $p < 0.01$, *** $p < 0.001$, **** $p < 0.0001$.

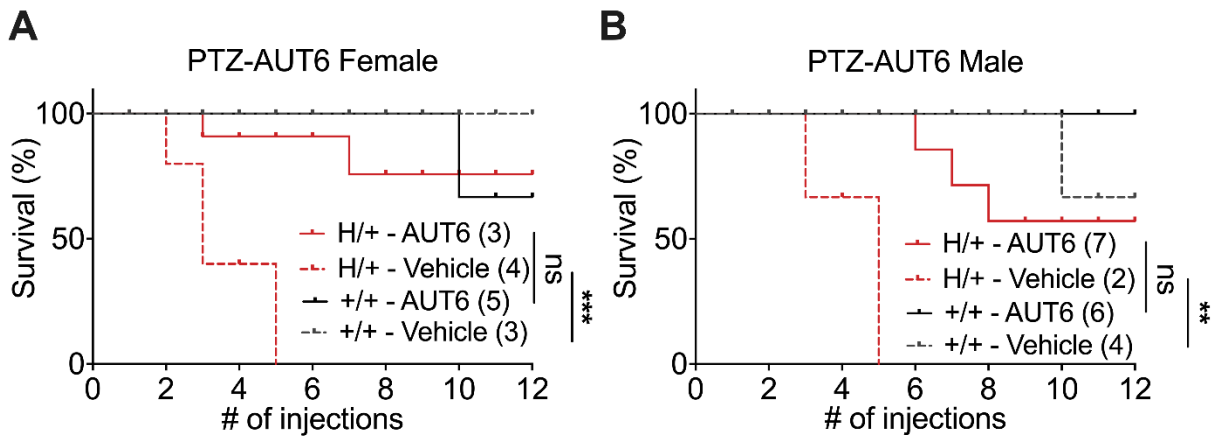


**Figure S11. The effect of AUT00206 on kindling epileptogenesis in H/+ mice persists in both male and female mice.** Related to Figure 6.

Treatment of AUT00206 eliminates the difference between H/+ and +/+ groups in both female (A) and male (B) mice.

Mantel-Cox Test;**, $p < 0.01$; ***, $p < 0.001$.

**Table S1** appears in a separate Excel file.

| | | | | Intrinsic Membrane Properties | | | | |
|---|---|---|---|---|---|---|---|---|
| Genotype | Age | Mice (*N*) | Cells (*n*) | $V_m$ | $R_m$ | Tau | Sag | Rheobase |
| | | | | mV | MOhms | ms | % | pA |
| H/H | P16-21 | 3 | 19 | -69.8 ± 2.4 | 1820 ± 258 | 12.8 ± 1.5 | 6 ± 1** | 19.6 ± 3.1 |
| H/+ | P16-21 | 4 | 39 | -78.6 ± 2.3 | 2376 ± 219 | 16.2 ± 1.7 | 12 ± 2* | 16.3 ± 2.2 |
| | 2-mo | 3 | 23 | -81.0 ± 1.5 | 1314 ± 150 | 9.82 ± 1.06 | 11 ± 2 | 25.6 ± 3.5 |
| | 4-mo | 2 | 20 | -80.9 ± 1.9 | 1109 ± 151 | 8.72 ± 0.81 | 14 ± 2 | 40.6 ± 5.1* |
| | 6-mo | 13 | 50 | -75.1 ± 1.6 | 2068 ± 173 | 13.9 ± 1.1 | 12 ± 1 | 19.4 ± 2.2 |
| +/+ | P16-21 | 4 | 39 | -72.1 ± 2.0 | 1676 ± 222 | 12.7 ±1.4 | 22 ± 4 | 15.5 ± 1.5 |
| | 2-mo | 3 | 23 | -81.4 ± 1.9 | 1267 ± 113 | 10.6 ± 1.2 | 13 ± 2 | 29.5 ± 2.8 |
| | 4-mo | 2 | 20 | -79.3 ± 1.3 | 1189 ± 137 | 9.40 ± 1.46 | 12 ± 1 | 25.1 ± 2.9 |
| | 6-mo | 13 | 40 | -78.1 ± 1.9 | 2593 ± 286 | 15.1 ± 1.5 | 9 ± 1 | 17.1 ± 2.9 |
| *p* values (via via One-way ANOVA or unpaired Student's t-test, vs. age-matched +/+ mice) | | | | | | | | |
| P16-21 | H/H vs. +/+ | | | 0.809 | 0.898 | 0.999 | 0.002 | 0.417 |
| P16-21 | H/+ vs. +/+ | | | 0.106 | 0.052 | 0.237 | 0.016 | 0.952 |
| 2-mo | H/+ vs. +/+ | | | 0.878 | 0.802 | 0.641 | 0.565 | 0.377 |
| 4-mo | H/+ vs. +/+ | | | 0.474 | 0.697 | 0.679 | 0.419 | 0.042 |
| 6-mo | H/+ vs. +/+ | | | 0.230 | 0.105 | 0.535 | 0.204 | 0.536 |

**Table S2. Intrinsic membrane properties of cerebellar granule cells by genotype and age.** Related to Figure 4.

*, $p < 0.05$; **, $p < 0.01$; ***, $p < 0.001$

| | | | | Action Potential Properties | | | | | | | | | | |
|---|---|---|---|---|---|---|---|---|---|---|---|---|---|---|
| Group | Age | Mice (*N*) | Cells (*n*) | Inflection Rate | Max Rise Slope | AP Thres-hold | AP Amp-litude | AP Peak | AP Rise Time | AP Halfwidth | AHP Amp-litude | AHP Time | ISI CoV |
| | | | | mV/ms | mV/ms | mV | mV | mV | ms | ms | mV | ms | |
| H/H | P16-21 | 3 | 19 | 12.9 ± 2.6* | 435 ± 44* | -45.2 ±1.2 | 71.5 ± 3.1* | 26.3 ± 3.0 | 0.62 ± 0.06 | 0.44 ± 0.02*** | -21.4 ± 0.8* | 2.0 ± 0.36*** | 0.39 ± 0.06** |
| H/+ | P16-21 | 4 | 39 | 18.5 ± 2.6 | 346 ± 20 | -42.9 ± 0.6 | 66.3 ± 1.8 | 23.4 ± 1.9 | 0.57 ± 0.02 | 0.40 ± 0.01* | -23.3 ± 0.6 | 1.42 ± 0.08 | 0.26 ± 0.03** |
| | 2-mo | 3 | 23 | 20.5 ± 4.1 | 392 ± 18*** | -45.7 ± 0.9 | 67.5 ± 1.4*** | 21.8 ± 1.5*** | 0.63 ± 0.05 | 0.34 ± 0.01** | -25.1 ± 0.5 | 1.24 ± 0.05*** | 0.22 ± 0.03* |
| | 4-mo | 2 | 22 | 20.9 ± 4.6 | 337 ± 18** | -42.0 ± 1.1 | 64.3 ± 1.7*** | 22.3 ± 1.7*** | 0.62 ± 0.05 | 0.38 ± 0.01* | -26.4 ± 1.0 | 1.31 ± 0.06** | 0.29 ± 0.05 |
| | 6-mo | 13 | 50 | 18.9 ± 2.4 | 296 ± 15* | -42.2 ± 0.7 | 61.7 ± 1.7* | 19.5 ± 1.5* | 0.62 ± 0.03 | 0.40 ± 0.01* | -25.9 ± 0.5 | 1.48 ± 0.06*** | 0.26 ± 0.03 |
| +/+ | P16-21 | 4 | 39 | 28.7 ± 5.3 | 333 ± 20 | -42.4 ±1.1 | 63.7 ± 1.9 | 21.2 ± 1.9 | 0.53 ± 0.04 | 0.34 ± 0.02 | -24.3 ± 0.7 | 1.01 ± 0.04 | 0.21 ± 0.02 |
| | 2-mo | 3 | 23 | 24.6 ± 3.4 | 285 ± 10 | -44.2 ± 0.8 | 54.4 ± 1.4 | 10.2 ± 1.4 | 0.57 ± 0.03 | 0.31 ± 0.01 | -26.5 ± 0.7 | 1.01 ± 0.04 | 0.16 ± 0.02 |
| | 4-mo | 2 | 22 | 18.6 ± 3.8 | 271 ± 15 | -43.1 ± 1.3 | 54.7 ± 1.7 | 11.6 ± 2.0 | 0.51 ± 0.03 | 0.34 ± 0.01 | -25.8 ± 0.8 | 1.08 ± 0.03 | 0.17 ± 0.03 |
| | 6-mo | 13 | 50 | 21.3 ± 3.1 | 249 ± 9 | -42.9 ± 1.0 | 57.4 ± 1.2 | 14.5 ± 1.2 | 0.62 ± 0.03 | 0.36 ± 0.01 | -24.8 ± 0.6 | 1.20 ± 0.04 | 0.24 ± 0.03 |
| *p* values (via via One-way ANOVA or unpaired Student's t-test, vs. age-matched +/+ mice) | | | | | | | | | | | | | |
| P16-21 | H/H vs. +/+ | | | 0.017 | 0.028 | 0.112 | 0.044 | 0.236 | 0.240 | 0.001 | 0.024 | <0.0001 | 0.002 |
| P16-21 | H/+ vs. +/+ | | | 0.075 | 0.902 | 0.900 | 0.556 | 0.668 | 0.718 | 0.020 | 0.477 | 0.002 | 0.497 |
| 2-mo | H/+ vs. +/+ | | | 0.440 | <0.0001 | 0.236 | <0.0001 | <0.0001 | 0.309 | 0.004 | 0.157 | 0.0004 | 0.035 |
| 4-mo | H/+ vs. +/+ | | | 0.706 | 0.007 | 0.498 | 0.0003 | 0.0002 | 0.060 | 0.017 | 0.655 | 0.0020 | 0.052 |
| 6-mo | H/+ vs. +/+ | | | 0.522 | 0.015 | 0.558 | 0.049 | 0.015 | 0.977 | 0.015 | 0.192 | 0.0007 | 0.550 |

**Table S3. Action potential properties of cerebellar granule cells by genotype and age.** Related to Figure 4.

*, $p < 0.05$; **, $p < 0.01$; ***, $p < 0.001$

| | | | | Firing Frequency | |
|---|---|---|---|---|---|
| Genotype | Age | Mice (*N*) | Cells (*n*) | Steady-state | Instantaneous |
| | | | | Hz | Hz |
| H/H | P16-21 | 3 | 19 | 95 ± 9**** | 141 ± 8**** |
| H/+ | P16-21 | 4 | 39 | 149 ± 6* | 175 ± 6 |
| | 2-mo | 3 | 23 | 134 ± 11*** | 174 ± 9*** |
| | 4-mo | 2 | 22 | 100 ± 9*** | 148 ± 6*** |
| | 6-mo | 13 | 50 | 101 ± 6*** | 138 ± 5*** |
| +/+ | P16-21 | 4 | 39 | 171 ± 7 | 199 ±7 |
| | 2-mo | 3 | 23 | 187 ± 8 | 228 ± 8 |
| | 4-mo | 2 | 22 | 172 ± 10 | 213 ± 7 |
| | 6-mo | 13 | 50 | 161 ± 7 | 195 ± 7 |
| *p* values (via via One-way ANOVA or unpaired Student's t-test, vs. age-matched +/+ mice) | | | | | |
| P16-21 | H/H vs. +/+ | | | <0.0001 | <0.0001 |
| P16-21 | H/+ vs. +/+ | | | 0.0406 | 0.058 |
| 2-mo | H/+ vs. +/+ | | | 0.0002 | <0.0001 |
| 4-mo | H/+ vs. +/+ | | | <0.0001 | <0.0001 |
| 6-mo | H/+ vs. +/+ | | | <0.0001 | <0.0001 |

**Table S4. Firing frequency of cerebellar granule cells by genotype and age.** Related to Figure 4.

*, $p < 0.05$; **, $p < 0.01$; ***, $p < 0.001$

| | | | | | Intrinsic Membrane Properties | | | | |
|---|---|---|---|---|---|---|---|---|---|
| Genotype | Age | Mice (*N*) | Cells (*n*) | $V_m$ | $R_m$ | Tau | Capacitance | Sag | Rheobase |
| | | | | mV | MOhms | ms | pF | % | pA |
| H/H | P16-21 | 3 | 11 | -71.2 ± 1.0 | 103 ± 8 | 7.7 ± 0.5 | 76.7 ± 5.1 | 6.2 ± 2.9 | 200 ± 36 |
| H/+ | P16-21 | 5 | 22 | -71.4 ± 1.2** | 99.3 ± 7.6 | 7.7 ± 0.9 | 86.5 ± 14.1 | 11.2 ± 1.5 | 200 ± 21 |
| | 6-mo | 3 | 29 | -64.3 ± 1.3** | 149 ± 11* | 10.3 ± 1.0** | 76.6 ± 8.7 | 14.3 ± 2.4 | 169 ± 21 |
| +/+ | P16-21 | 3 | 13 | -76.5 ± 1.1 | 112 ± 8 | 5.3 ± 0.6 | 68.6 ± 6.3 | 7.8 ± 0.7 | 177 ± 24 |
| | 6-mo | 3 | 25 | -70.0 ± 1.7 | 112 ± 9 | 5.9 ± 0.4 | 57.9 ± 4.9 | 9.2 ± 1.1 | 180 ± 15 |
| | *p* values (via via One-way ANOVA or unpaired Student's t-test, vs. age-matched +/+ mice) | | | | | | | | |
| P16-21 | H/H vs. +/+ | | | 0.0178 | 0.7017 | 0.2494 | 0.8839 | 0.7931 | 0.7986 |
| P16-21 | H/+ vs. +/+ | | | 0.0067 | 0.4076 | 0.0641 | 0.4668 | 0.2846 | 0.7373 |
| 6-mo | H/+ vs. +/+ | | | 0.009 | 0.014 | 0.0003 | 0.0786 | 0.0655 | 0.6966 |

**Table S5. Intrinsic membrane properties of neocortex PV+ GABAergic interneurons by genotype and age.** Related to Figure 5.

*, $p < 0.05$; **, $p < 0.01$; ***, $p < 0.001$

| | | | | Action Potential Properties | | | | | | | |
|---|---|---|---|---|---|---|---|---|---|---|---|
| Group | Age | Mice (*N*) | Cells (*n*) | Max Rise Slope | AP Thres-hold | AP Amp-litude | AP Peak | AP Rise Time | AP Halfwidth | AHP Amp-litude | AHP Time |
| | | | | mV/ms | mV | mV | mV | ms | ms | mV | ms |
| H/H | P16-21 | 3 | 11 | 421 ± 69 | -45.1 ± 1.2 | 66.2 ± 5.1 | 21.1 ± 4.1 | 0.355 ± 0.033 | 0.40 ± 0.04** | -26.4 ± 1.0 | 1.9 ± 0.2*** |
| H/+ | P16-21 | 5 | 22 | 393 ± 30 | -45.2 ± 0.9 | 62.0 ± 1.8 | 16.9 ± 1.9 | 0.317 ± 0.020 | 0.31 ± 0.02 | -28.7 ± 1.0 | 1.3 ± 0.1 |
| | 6-mo | 3 | 29 | 550 ± 54** | -42.1 ± 1.1 | 77.6 ± 2.4*** | 35.4 ± 3.0*** | 0.376 ± 0.033 | 0.39 ± 0.04* | -26.7 ± 1.3*** | 2.0 ± 0.1*** |
| +/+ | P16-21 | 3 | 13 | 439 ± 36 | -47.9 ± 0.4 | 68.0 ± 2.7 | 20.1 ± 2.5 | 0.302 ± 0.015 | 0.30 ± 0.01 | -27.9 ± 1.3 | 1.2 ± 0.1 |
| | 6-mo | 3 | 25 | 360 ± 33 | -42.1 ± 1.6 | 62.0 ± 2.3 | 19.9 ± 2.4 | 0.349 ± 0.014 | 0.29 ± 0.01 | -26.2 ± 0.9 | 1.0 ± 0.04 |
| *p* values (via via One-way ANOVA or unpaired Student's t-test, vs. age-matched +/+ mice) | | | | | | | | | | | |
| P16-21 | H/H vs. +/+ | | | 0.9494 | 0.1672 | 0.8927 | 0.9639 | 0.2487 | 0.0079 | 0.6153 | 0.0004 |
| P16-21 | H/+ vs. +/+ | | | 0.6406 | 0.0933 | 0.2289 | 0.5571 | 0.8492 | 0.8775 | 0.8304 | 0.996 |
| 6-mo | H/+ vs. +/+ | | | 0.006 | 0.9919 | <0.0001 | 0.0002 | 0.4809 | 0.025 | <0.0001 | <0.0001 |

**Table S6. Action potential properties of neocortex PV+ GABAergic interneurons by genotype and age.**
Related to Figure 5.

*, $p < 0.05$; **, $p < 0.01$; ***, $p < 0.001$

| | | | | Firing Frequency | |
|---|---|---|---|---|---|
| Genotype | Age | Mice (*N*) | Cells (*n*) | Steady-state | Instantaneous |
| | | | | Hz | Hz |
| H/H | P16-21 | 3 | 11 | 226 ± 14** | 246 ± 12*** |
| H/+ | P16-21 | 5 | 22 | 283 ± 10 | 314 ± 10 |
| | 6-mo | 3 | 29 | 199 ± 22*** | 245 ± 24*** |
| +/+ | P16-21 | 3 | 13 | 294 ± 14 | 327 ± 15 |
| | 6-mo | 3 | 25 | 318 ± 12 | 401 ± 13 |
| *p* values (via via One-way ANOVA or unpaired Student's t-test, vs. age-matched +/+ mice) | | | | | |
| P16-21 | H/H vs. +/+ | | | 0.0018 | 0.0004 |
| P16-21 | H/+ vs. +/+ | | | 0.7449 | 0.680 |
| 6-mo | H/+ vs. +/+ | | | <0.0001 | <0.0001 |

**Table S7. Firing frequency of neocortex PV+ GABAergic interneurons by genotype and age.**
Related to Figure 5.

*, $p < 0.05$; **, $p < 0.01$; ***, $p < 0.001$

| | | | | Intrinsic Membrane Properties | | | | |
|---|---|---|---|---|---|---|---|---|
| Brain Region | Genotype | Mice (*N*) | Cells (*n*) | $V_m$ | $R_m$ | Tau | Sag | Rheobase |
| | | | | mV | MOhms | ms | % | pA |
| CA3 | H/+ | 5 | 17 | -55.1 ± 1.2 | 84.3 ± 11.0 | 9.5 ± 0.9 | 33 ± 5** | 186 ± 18 |
| | +/+ | 3 | 8 | -54.8 ± 1.5 | 159 ± 43 | 10.6 ± 1.1 | 11 ± 2 | 160 ± 24 |
| RTN | H/+ | 4 | 34 | -59.6 ± 2.4 | 230 ± 15 | 14.4 ± 0.9 | 7 ± 1 | 59 ± 8 |
| | +/+ | 3 | 13 | -57.9 ± 2.6 | 428 ± 70 | 14.9 ± 1.3 | 5 ± 1 | 44 ± 13 |
| IC | H/+ | 2 | 25 | -61.0 ± 1.1 | 84.2 ± 15.8 | 5.1 ± 0.6 | 169 ± 18 | 161 ± 20 |
| | +/+ | 2 | 24 | -61.8 ± 1.1 | 62.9 ± 13.6 | 4.0 ± 0.3 | 178 ± 23 | 203 ± 21 |
| *p* values (via via One-way ANOVA or unpaired Student's t-test, vs. age-matched +/+ mice) | | | | | | | | |
| CA3 | | | | 0.894 | 0.169 | 0.500 | 0.002 | 0.452 |
| RTN | | | | 0.158 | 0.009 | 0.374 | 0.648 | 0.969 |
| IC | | | | 0.595 | 0.313 | 0.111 | 0.766 | 0.153 |

**Table S8. Intrinsic membrane properties of Kv3.1-expressing PV+ neurons in H/+ vs. wild-type mice.** Related to Figure 5.

*, $p < 0.05$; **, $p < 0.01$; ***, $p < 0.001$. CA3, hippocampal CA3; IC, inferior colliculus; RTN, thalamic reticular nucleus. All recordings performed at P16-21.

| | | | | Action Potential Properties | | | | | | | | | |
|---|---|---|---|---|---|---|---|---|---|---|---|---|---|
| Group | Age | Mice (N) | Cells (n) | Inflection Rate | Max Rise Slope | AP Thres-hold | AP Amp-litude | AP Peak | AP Rise Time | AP Halfwidth | AHP Amp-litude | AHP Time | ISI CoV |
| | | | | mV/ms | mV/ms | mV | mV | mV | ms | ms | mV | ms | |
| CA3 | H/+ | 5 | 17 | 12.1 ± 2.6 | 664 ± 60** | -44.4 ± 1.5 | 86.8 ± 3.3* | 42.3 ± 2.6* | 0.50 ± 0.03 | 0.34 ± 0.02 | -18.4 ± 1.1 | 1.00 ± 0.11 | 0.18 ± 0.03 |
| | +/+ | 3 | 8 | 26.4 ± 6.7 | 457 ± 25 | -44.2 ± 1.9 | 75.7 ± 2.9 | 31.5 ± 3.0 | 0.44 ± 0.03 | 0.32 ± 0.01 | -18.8 ± 1.7 | 0.84 ± 0.03 | 0.21 ± 0.05 |
| RTN | H/+ | 4 | 34 | 15.2 ± 2.1 | 491 ± 32 | -42.8 ± 0.5* | 80.8 ± 1.9 | 38.1 ± 1.8 | 0.62 ± 0.05 | 0.39 ± 0.03 | -15.5 ± 0.8 | 1.05 ± 0.08 | 0.26 ± 0.02*** |
| | +/+ | 3 | 13 | 25.5 ± 5.7 | 452 ± 29 | -40.3 ± 2.0 | 79.8 ± 3.1 | 39.5 ± 2.6 | 0.54 ± 0.06 | 0.38 ± 0.02 | -16.5 ± 1.6 | 1.30 ± 0.32 | 0.17 ± 0.02 |
| IC | H/+ | 2 | 25 | 5.5 ± 0.7 | 222 ± 9 | -41.2 ± 0.9 | 53.5 ± 1.5 | 12.3 ± 1.9 | 0.67 ± 0.02 | 0.38 ± 0.02 | -19.4 ± 0.8 | 1.02 ± 0.14 | 0.24 ± 0.03 |
| | +/+ | 2 | 24 | 4.0 ± 0.4 | 238 ± 6 | -42.9 ± 1.0 | 55.6 ± 1.2 | 12.7 ± 1.2 | 0.73 ± 0.04 | 0.36 ± 0.02 | -16.9 ± 1.0 | 0.74 ± 0.05 | 0.33 ± 0.03 |
| *p* values (via via One-way ANOVA or unpaired Student's t-test, vs. age-matched +/+ mice) | | | | | | | | | | | | | |
| CA3 | | | | 0.110 | 0.008 | 0.922 | 0.030 | 0.026 | 0.292 | 0.369 | 0.883 | 0.197 | 0.645 |
| RTN | | | | 0.143 | 0.762 | 0.040 | 0.890 | 0.286 | 0.570 | 0.777 | 0.065 | 0.415 | 0.0002 |
| IC | | | | 0.070 | 0.139 | 0.239 | 0.279 | 0.839 | 0.244 | 0.458 | 0.059 | 0.082 | 0.0637 |

**Table S9. Action potential properties of Kv3.1-expressing PV+ neurons in H/+ vs. wild-type mice.** Related to Figure 4-5.

*, $p < 0.05$; **, $p < 0.01$; ***, $p < 0.001$. CA3, hippocampal CA3; IC, inferior colliculus; RTN, thalamic reticular nucleus. All recordings performed at P16-21.

| | | | | Firing Frequency | |
|---|---|---|---|---|---|
| Group | Age | Mice (*N*) | Cells (*n*) | Steady-state | Instantaneous |
| | | | | Hz | Hz |
| CA3 | H/+ | 5 | 17 | 219 ± 13 | 286 ± 18 |
| | +/+ | 3 | 8 | 253 ± 16 | 319 ± 13 |
| RTN | H/+ | 4 | 34 | 178 ± 10 | 287 ± 10 |
| | +/+ | 3 | 13 | 209 ± 13 | 300 ± 15 |
| IC | H/+ | 2 | 25 | 259 ± 20 | 385 ± 17* |
| | +/+ | 2 | 24 | 288 ± 26 | 442 ± 12 |
| CA3 | | | | 0.163 | 0.183 |
| RTN | | | | 0.175 | 0.889 |
| IC | | | | 0.380 | 0.010 |

**Table S10. Firing frequency of Kv3.1-expressing PV+ neurons in H/+ vs. wild-type mice.** Related to Figure 4-5.

*, $p < 0.05$; **, $p < 0.01$; ***, $p < 0.001$. CA3, hippocampal CA3; IC, inferior colliculus; RTN, thalamic reticular nucleus. All recordings performed at P16-21.